Contracting bubbles in Hele-Shaw cells with a power-law fluid

Scott W McCue[1] **and John R King**[2]

[1] Mathematical Sciences, Queensland University of Technology, Brisbane QLD 4001, Australia

[2] School of Mathematical Sciences, University of Nottingham, Nottingham NG7 2RD, UK

E-mail: scott.mccue@qut.edu.au, john.king@nottingham.ac.uk

Abstract. The problem of bubble contraction in a Hele-Shaw cell is studied for the case in which the surrounding fluid is of power-law type. A small perturbation of the radially symmetric problem is first considered, focussing on the behaviour just before the bubble vanishes, it being found that for shear-thinning fluids the radially symmetric solution is stable, while for shear-thickening fluids the aspect ratio of the bubble boundary increases. The borderline (Newtonian) case considered previously is neutrally stable, the bubble boundary becoming elliptic in shape with the eccentricity of the ellipse depending on the initial data. Further light is shed on the bubble contraction problem by considering a long thin Hele-Shaw cell: for early times the leading-order behaviour is one-dimensional in this limit; however, as the bubble contracts its evolution is ultimately determined by the solution of a Wiener-Hopf problem, the transition between the long-thin limit and the extinction limit in which the bubble vanishes being described by what is in effect a similarity solution of the second kind. This same solution describes the generic (slit-like) extinction behaviour for shear-thickening fluids, the interface profiles that generalise the ellipses that characterise the Newtonian case being constructed by the Wiener-Hopf calculation.

Mathematics Subject Classification 35B40, 35R35, 76D27

Submitted to: *Nonlinearity*

1. Introduction

The flow of a Newtonian fluid in a Hele-Shaw cell has been the subject of a great deal of study, in part because it serves as a two-dimensional analogue of saturated flow through a porous medium. Indeed, the task of performing accurate experiments is much less demanding in Hele-Shaw cells than it is in porous media, especially when the system involves a moving interface between two different fluids. From a mathematical perspective these flows are governed by Laplace's equation in the flow domain, with any interface modelled as a free boundary. The result is a free boundary problem which has received an enormous amount of attention in the literature (see, for example, the long list of references on the web site [41]). As further motivations, we note that solidification processes in which the latent heat of fusion is large compared to the sensible heat are described in the limit by the same free boundary problem as for Newtonian Hele-Shaw flow and, more relevant to the current study, the Hele-Shaw problem serves as a paradigm for injection moulding.

This paper is concerned with bubbles of air in Hele-Shaw cells which are otherwise filled with non-Newtonian fluid. Examples of non-Newtonian fluids include liquid crystals, polymer melts and some foams, with related problems in Hele-Shaw flow being studied in [2, 3, 11, 23, 24, 28, 30, 31, 35, 36, 40], for instance. Some of these works concern applications to injection moulding, many of the fluids typically used in such contexts having shear-thinning properties and our focus here is on power-law fluids.

The class of non-Newtonian fluids with which we shall be concerned has viscosity μ dependent on the rate-of-strain tensor $\mathbf{D}$. In the present study we shall assume the fluid's viscosity varies according to the power-law relationship

$$\mu = k\|\mathbf{D}\|^{m-1},$$

where $\|\mathbf{D}\| = \sqrt{\mathbf{D} : \mathbf{D}}$, with the colon denoting an inner product. Here k and m are (positive) material constants, with $m < 1$ corresponding to a shear-thinning fluid, $m > 1$ to a shear-thickening fluid, and $m = 1$ to a Newtonian fluid. Ignoring inertia and body forces, the equation of motion is $\boldsymbol{\nabla} p = \operatorname{div}(2\mu\mathbf{D})$, where p is the fluid pressure. By carefully averaging over the small gap between the plates in the Hele-Shaw cell, and by satisfying conservation of mass, we can eliminate the components of velocity from the problem. As a result, the governing equation for Hele-Shaw flow of such a power-law fluid is the (nonlinear) p-harmonic[3] equation

$$\boldsymbol{\nabla} \cdot \left(|\boldsymbol{\nabla} p|^{(1-m)/m} \boldsymbol{\nabla} p \right) = 0, \tag{1}$$

where the operator $\boldsymbol{\nabla}$ is two-dimensional with independent variables $\mathbf{x} = (x, y)$. For a full derivation of (1), see Aronsson & Janfalk [11] or Hieber & Shen [24]. Of course, for the Newtonian case $m = 1$ our governing equation (1) reduces to Laplace's equation. If

[3] The p in 'p-harmonic' of course relates to the exponent $p = (m + 1)/m$, rather than to the fluid pressure.

there is a uniform-pressure bubble in the Hele-Shaw cell occupying the space $\Omega(t)$, then we have the boundary conditions

$$p = 0, \quad V_n = -|\boldsymbol{\nabla} p|^{(1-m)/m} \frac{\partial p}{\partial n} \tag{2}$$

on the bubble boundary $\partial\Omega$, where $\partial/\partial n$ is the normal derivative and V_n the normal velocity of the moving interface, directed into Ω.

It is well known that if a bubble is injected into a Hele-Shaw cell filled with a Newtonian viscous fluid then fingering can occur, a phenomenon referred to as the Saffman-Taylor instability [37]. Conversely, the reverse process, whereby the bubble is forced to contract by the extraction of air, is stable, with the bubble ultimately shrinking smoothly to a point (or points, if it subdivides prior to extinction). The current study is primarily concerned with the latter process; in particular, we wish to examine the behaviour of the flow field and the shape of the bubble at times just before the bubble vanishes (i.e. just before the mould is filled). In terms of injection moulding, the shrinking bubble problem is of practical importance. In particular, it could be important to know in advance the location of the point at which the bubble vanishes, as this is where the air vents or outlets should be placed to prevent unwanted air bubbles in the mould. Furthermore, bubbles with very large aspect ratios could lead to mechanical weaknesses, and thus knowledge of this limiting behaviour is instructive.

The corresponding problem for a Newtonian fluid is treated in Entov & Etingof [17] and McCue *et al.* [32]. There it is shown that the bubble shape becomes elliptic just before the bubble vanishes, and has an aspect ratio that depends on the initial geometry (such behaviour has interesting relations to the mathematical theory of quadrature domains [15, 21, 38]; specifically, the elliptic shape is associated with null quadrature domains [18, 26]). The present aim is to extend these results to power-law fluids and, in particular, to determine the effect of varying the index m. Note that related studies of solidification problems are undertaken in [6, 33, 34, 39], for example. However, the power-law Hele-Shaw problem differs from all of these previous studies in that no Baiocchi transform is available, this having significant implications for the analysis; indeed, that the power-law Hele-Shaw problem is one of the simplest that lacks this property (cf. [28]) provides a further motivation for the current work, yet another being provided by the widely-studied focusing (or hole-filling) problem for the porous medium equation

$$\frac{\partial u}{\partial t} = \boldsymbol{\nabla} \cdot (u^\gamma \boldsymbol{\nabla} u) \quad \text{outside} \quad \Omega(t); \quad u = u^\gamma \frac{\partial u}{\partial n} = 0 \quad \text{on} \quad \partial\Omega. \tag{3}$$

In this problem an initial (positive) distribution for u (which corresponds to a viscous gravity current for the case $\gamma = 3$) exists outside a closed region $\Omega(0)$ in the plane, with $u = 0$ inside $\Omega(0)$ (the hole). For $t > 0$ the hole fills, and $\Omega(t)$ 'focuses' to a point at some finite time t_e. It is known that for $0 < \gamma < \infty$ the aspect ratio of the interface $\partial\Omega(t)$ generically becomes unbounded as $t \to t_e$, implying that Ω becomes a slit in shape just before 'extinction' (see [8, 9, 10, 14]). However, the limiting case $\gamma = \infty$ corresponds to the Newtonian Hele-Shaw problem, for which it is known that $\partial\Omega(t)$

becomes elliptic in shape in that limit, as described above. Thus the current Hele-Shaw problem for a power-law fluid provides a more instructive paradigm in the sense that we can investigate both sides of the critical case (namely $m = 1$ in (1) but $\gamma = \infty$ in (3)).

The paper is organised as follows. Section 2 contains some preliminary analysis. In section 3, we formulate the problem in question, and make note of the key differences between the solution for shear-thinning and shear-thickening cases at the precise moment the bubbles vanishes (at extinction). We then consider the radially symmetric solution to the problem and study the effect of slightly perturbing the geometry, paying particular attention to the behaviour just before extinction. The analysis reveals the exceptional nature of the Newtonian case $m = 1$, which in this context (with shrinking bubbles) provides a distinct borderline between stable ($0 < m < 1$) and unstable ($m > 1$) radially symmetric solutions; the former suggests that for the shear-thinning case ($m < 1$) the near extinction behaviour is radially symmetric. This classification is further explored in section 4, in which the bubble contraction problem is treated for a long, thin Hele-Shaw cell. For this geometry the key features of the near extinction limit can be described by a Wiener-Hopf problem, the solution of which again identifies the borderline nature of the Newtonian case. The analysis predicts that for the shear-thickening case ($m > 1$) the bubbles ultimately stretch out and approach a slit in shape, while for the shear-thinning case ($m < 1$) the thin bubble fattens up and, on a further time-scale, evolves to a circular shape. The implications of these results for general (i.e. $\mathcal{O}(1)$-aspect-ratio) domains is then described in section 5. Finally, the paper is closed in section 6 with a discussion.

2. Formulation and extinction-time behaviour

2.1. Preamble

Consider a Hele-Shaw cell which covers a finite region B, and whose boundary is denoted by ∂B. We suppose there is a contracting bubble which occupies the region $\Omega(t)$ ($\Omega(t) \subseteq B$), with the remainder of the cell filled with a non-Newtonian fluid of power-law type. It follows that we must solve (1) in $B \setminus \Omega(t)$, subject to the free boundary conditions (2) on $\partial\Omega$. If we suppose for simplicity that the bubble contraction is forced by fluid injected at constant pressure at the boundary ∂B, then we also have

$$p = 1 \quad \text{on} \quad \partial B. \tag{4}$$

The initial condition we adopt is that at $t = 0$, $\partial\Omega$ coincides with ∂B. We note that the boundary conditions chosen above are typically not the most appropriate ones in applications to injection moulding, where instead the process may be driven by sources or sinks within the flow domain, or perhaps by a Neumann condition at the fixed boundary ∂B. However, we are most interested in the flow characteristics in the neighbourhood of the point where the bubble vanishes, and conjecture that the associated limiting behaviour will hold regardless of the driving mechanism behind the flow field (indeed,

the boundary value problems derived below that govern the behaviour near extinction do not depend in detail on the conditions on ∂B).

A summary of the known results for this problem in the case of a Newtonian fluid ($m = 1$), taken from [17, 32, 33], is presented in Appendix A.

2.2. Behaviour at extinction

There is a striking difference between the behaviour at extinction (i.e. at $t = t_e$) of the shear-thinning and shear-thickening cases (post-extinction we simply have $p \equiv 1$ for all m), which we now record and which will be crucial in the analysis that follows.

Taking extinction to occur at time $t = t_e$ and location $(x, y) = (x_e, y_e) = \mathbf{x}_e$, for $m \geq 1$ we have throughout B that

$$p_e(x, y) = 1 \quad \text{for} \quad m \geq 1,$$

where $p_e(x, y) \equiv p(x, y, t_e)$, and

$$p(x, y, t) \sim 1 - \chi(t)\Phi(x, y) \quad \text{for} \quad (x, y) \neq (x_e, y_e), \quad m \geq 1, \tag{5}$$

where $\chi(t) \to 0^+$ as $t \to t_e^-$ (and subsequently needs to be determined as part of the solution; see section 6), while Φ is the 'Green's function'

$$\boldsymbol{\nabla} \cdot \left(|\boldsymbol{\nabla}\Phi|^{(1-m)/m} \boldsymbol{\nabla}\Phi \right) = 0 \quad \text{in} \quad B \setminus \{(x_e, y_e)\}, \tag{6}$$

$$\Phi = 0 \quad \text{on} \quad \partial B, \quad \Phi \sim \begin{cases} -\log r - K & \text{as} \quad r \to 0, \quad m = 1, \\ r^{-(m-1)} - K & \text{as} \quad r \to 0, \quad m > 1, \end{cases} \tag{7}$$

where $r = |\mathbf{x} - \mathbf{x}_e|$ and K is a constant that depends on B. (Note that, as a non-negative solution to the p-Laplace equation, Φ must be asymptotically radial as $r \to 0$ [27].)

In sharp contrast, for $m < 1$ we have instead that

$$\boldsymbol{\nabla} \cdot \left(|\boldsymbol{\nabla} p_e|^{(1-m)/m} \boldsymbol{\nabla} p_e \right) = 0 \quad \text{in} \quad B \setminus \{(x_e, y_e)\}, \tag{8}$$

$$p_e = 1 \quad \text{on} \quad \partial B, \quad p_e = 0 \quad \text{at} \quad r = 0, \tag{9}$$

with the local behaviour

$$p_e \sim A_e r^{1-m} \quad \text{as} \quad r \to 0 \tag{10}$$

for some positive constant A_e. Note that, as is well-known, a Dirichlet boundary condition can only be imposed on Laplace's equation at $r = 0$ if the dimension $N < 2$, so that here the shear-thinning case for $N = 2$ is behaving in a subcritical fashion; in higher dimensions the relevant behaviour would be

$$p_e \sim A_e r^{1-m(N-1)}, \quad m < 1/(N-1), \tag{11}$$

so, more generally, the critical exponent in N dimensions is the conformally-invariant one $m = 1/(N-1)$ (giving the N-Laplace equation).

3. The near-circular Hele-Shaw cell

3.1. Asymptotic solution

As part of the analysis in Appendix A, valid for $m = 1$, we detail a recipe for computing the extinction time t_e and extinction point $\mathbf{x}_e$ given any domain B, as well as the shape of the contracting bubble at times just before the bubble vanishes, these results being derived from the Baiocchi transform formulation. For the general case in which $m \neq 1$, the Baiocchi transform is not applicable, and thus a derivation of equivalent exact results is not possible (at least not for a general domain B).

To gain further understanding of the extinction behaviour for power-law fluids, it is instructive first to consider the stability of the radially symmetric solution to (1), (2) and (4), by studying the problem which arises if ∂B is slightly perturbed from a circle, and tracking the modes of perturbation as the bubble boundary evolves. To this end, we employ the usual polar coordinates (r, θ), write $p = p(r, \theta, t)$, and denote the bubble boundary by $r = s(\theta, t)$. Further, we assume ∂B is described by $r = 1 + \epsilon g(\theta)$, where $\epsilon \ll 1$, and g is the periodic function represented by

$$g(\theta) = \sum_{n=1}^{\infty} a_n \cos n\theta, \tag{12}$$

(we omit $\sin n\theta$ terms simply for brevity) and expand s and p in the form

$$p = p_0(r, t) + \epsilon\, p_1(r, \theta, t) + \mathcal{O}(\epsilon^2), \quad s = s_0(t) + \epsilon\, s_1(\theta, t) + \mathcal{O}(\epsilon^2). \tag{13}$$

The approach used to solve for p_0, s_0, p_1 and s_1 is straightforward; we list the solutions here, and relegate the details to Appendix B.

For $m = 1$ the solution for the leading order pressure field is

$$p_0 = 1 - \frac{\log r}{\log s_0}, \quad m = 1, \tag{14}$$

and the leading order free boundary description is

$$t = \tfrac{1}{4} + \tfrac{1}{2} s_0^2 \log s_0 - \tfrac{1}{4} s_0^2. \tag{15}$$

The extinction time for the radially symmetric problem is thus $t_{e0} = \frac{1}{4}$. With $m \neq 1$, we have

$$p_0 = \frac{r^{1-m} - s_0^{1-m}}{1 - s_0^{1-m}}, \quad m \neq 1. \tag{16}$$

For the shear-thinning case $m < 1$, the leading order free boundary $s_0(t)$ is given implicitly by

$$t_{e0} - t = \frac{1}{2(1-m)^{1/m}} s_0^2 F(-\tfrac{1}{m}, \tfrac{2}{1-m}; \tfrac{3-m}{1-m}; s_0^{1-m}),$$

where $F(a, b; c; z)$ is the usual hypergeometric function. Here t_{e0}, the extinction time for this leading-order problem, is given by

$$t_{e0} = \frac{\Gamma(\frac{3-m}{1-m})\Gamma(\frac{1+m}{m})}{2(1-m)^{1/m}\Gamma(\frac{1+2m-m^2}{m(1-m)})},$$

where $\Gamma(z)$ is the usual Gamma function. Note that

$$t_{e0} - t = \frac{1}{2(1-m)^{1/m}} \left\{ s_0^2 - \frac{2}{m(3-m)} s_0^{3-m} + \mathcal{O}(s_0^{2(2-m)}) \right\} \quad \text{as} \quad s_0 \to 0,$$

so that, to leading order,

$$s_0 \sim 2^{1/2}(1-m)^{1/2m}(t_{e0}-t)^{1/2} \quad \text{as} \quad t \to t_{e0}^-. \tag{17}$$

For the shear-thickening case $m > 1$, the leading-order free boundary is described by

$$t_{e0} - t = \frac{m}{(1+m)(m-1)^{1/m}} s_0^{(1+m)/m} F(-\tfrac{1}{m}, \tfrac{1+m}{m(1-m)}; \tfrac{1+m^2}{m(1-m)}; s_0^{m-1}),$$

with the extinction time for the leading-order problem given by

$$t_{e0} = \frac{m\Gamma(\frac{1+m^2}{m(m-1)})\Gamma(\frac{m+1}{m})}{(1+m)(m-1)^{1/m}\Gamma(\frac{m+1}{m-1})}.$$

We have the limiting behaviour

$$t_{e0} - t = \frac{m}{(1+m)(m-1)^{1/m}} \left\{ s_0^{\frac{1+m}{m}} - \tfrac{1+m}{m(1+m^2)} s_0^{\frac{1+m^2}{m}} + O\left(s_0^{\frac{1-m+2m^2}{m}} \right) \right\}$$

as $s_0 \to 0$, so that, to leading order,

$$s_0 \sim \left[\frac{(1+m)(m-1)^{1/m}}{m} \right]^{m/(1+m)} (t_{e0}-t)^{m/(1+m)} \quad \text{as} \quad t \to t_{e0}^-. \tag{18}$$

Note how the temporal scaling here is dependent on m, in contrast to the shear-thinning case (17).

The solutions for the corrections terms can be written as

$$p_1(r,\theta,t) = \sum_{n=1}^{\infty} \phi_n(r,t)\cos n\theta, \quad s_1(\theta,t) = \sum_{n=1}^{\infty} \sigma_n(t)\cos n\theta, \tag{19}$$

where

$$\phi_n = A_n(t) r^{\nu+\mu_n} + B_n(t) r^{\nu-\mu_n}, \tag{20}$$

$$\nu = \tfrac{1}{2}(1-m), \quad \mu_n = \tfrac{1}{2}\sqrt{m^2 + 2(2n^2-1)m + 1}, \tag{21}$$

and for the Newtonian case $m = 1$

$$A_n = \frac{1}{s_0 \log s_0} \left(\frac{\sigma_n - a_n s_0^{1-n}}{s_0^n - s_0^{-n}} \right), \quad B_n = -\frac{1}{s_0 \log s_0} \left(\frac{\sigma_n - a_n s_0^{1+n}}{s_0^n - s_0^{-n}} \right),$$

while for $m \neq 1$

$$A_n = \frac{-(1-m)}{s_0^m(1-s_0^{1-m})} \left(\frac{\sigma_n - a_n s_0^{\nu-\mu_n+m}}{s_0^{\nu+\mu_n} - s_0^{\nu-\mu_n}} \right),$$

$$B_n = \frac{1-m}{s_0^m(1-s_0^{1-m})} \left(\frac{\sigma_n - a_n s_0^{\nu+\mu_n+m}}{s_0^{\nu+\mu_n} - s_0^{\nu-\mu_n}} \right).$$

Further,

$$\sigma_n = \frac{\mu_n a_n}{m\lambda_n s_0^{1+\frac{\nu}{m}}(s_0^{-\mu_n}-s_0^{\mu_n})^{\frac{1}{m}}}\left\{\frac{\Gamma(1+\frac{\lambda_n}{\mu_n})\Gamma(\frac{1}{m})}{\Gamma(\frac{\lambda_n}{\mu_n}+\frac{1}{m})} - s_0^{2\lambda_n}F(-\tfrac{1}{m}+1,\tfrac{\lambda_n}{\mu_n};1+\tfrac{\lambda_n}{\mu_n};s_0^{2\mu_n})\right\},$$

where the constant λ_n denotes the combination

$$\lambda_n = \tfrac{1}{2}\left[\nu+\mu_n+m+1+(\nu-\mu_n)/m\right].$$

Note that when $m=1$ we have $\nu=0$ and $\mu_n=n$, and in this case the σ_n simplify to

$$\sigma_1 = a_1, \quad \sigma_n = \frac{n a_n s_0^{n-1}(1-s_0^2)}{(1-s_0^{2n})} \quad \text{for} \quad n=2,3,\ldots.$$

3.2. Near-extinction behaviour

We note that as $s_0 \to 0$,

$$\sigma_n \sim \frac{\mu_n a_n}{m\lambda_n}\frac{\Gamma(1+\frac{\lambda_n}{\mu_n})\Gamma(\frac{1}{m})}{\Gamma(\frac{\lambda_n}{\mu_n}+\frac{1}{m})}\, s_0^{-1+(\mu_n-\nu)/m} \tag{22}$$

and, in particular, $\sigma_1 \to a_1$. Thus, σ_1 does not vanish in the extinction limit unless the perturbation is such that $a_1=0$ and, as with the Newtonian case discussed in Appendix A.4, it is evident that the a_1 mode affects the location of the extinction point: without any loss of generality we can choose the origin of $\mathbf{x}$ such that $a_1=0$ (this giving the 'optimal' choice for the origin), implying that $\sigma_1 \equiv 0$. (It is important to stress that a_1 is a property of the known domain boundary ∂B, not of the free boundary; (22) shows the choice $a_1=0$ achieves the desired goal of setting $\sigma_1=0$ at $t=t_e$ in the linearised problem.)

To analyse the aspect ratio of the evolving bubble, given by

$$\frac{s(0,t)}{s(\pi/2,t)} = 1+\epsilon\,\frac{s_1(0,t)-s_1(\pi/2,t)}{s_0(t)}+\mathcal{O}(\epsilon^2),$$

we use (22) to observe that

$$\frac{s_1(0,t)-s_1(\pi/2,t)}{s_0(t)} \sim \kappa_2 s_0^{-\delta} \quad \text{as} \quad s_0 \to 0,$$

where

$$\delta = \frac{3}{2}+\frac{1}{2m}(1-\sqrt{m^2+14m+1}), \quad \kappa_2 = \frac{2a_2\Gamma(\frac{1}{m})}{m}\left[\frac{\mu_2\Gamma(1+\frac{\lambda_2}{\mu_2})}{\lambda_2\Gamma(\frac{\lambda_2}{\mu_2}+\frac{1}{m})}\right]. \tag{23}$$

There are evidently three distinct regimes, which we now consider separately. Before proceeding, however, we note that we are most interested in the size of σ_n in the limit $s_0 \to 0$, with $\sigma_n = o(s_0)$) implying that the associated mode is stable (the perturbation decays faster than the leading order term vanishes). The aspect ratio $s(0,t)/s(\pi/2,t)$ is a further measure, with $s(0,t)/s(\pi/2,t) \to 1$ as $s_0 \to 0$ a requirement for stability (this is true regardless of whether or not $s(0,t)/s(\pi/2,t)$ is a ratio of the bubble's longest dimension to its shortest dimension).

For $m < 1$, the constant $\delta < 0$, and the aspect ratio of the free boundary

$$\frac{s(0,t)}{s(\pi/2,t)} \to 1 \quad \text{as} \quad s_0 \to 0.$$

Thus for the shear-thinning case $m < 1$ we infer that the bubble approaches a circle as it disappears. Here

$$\sigma_n = \mathcal{O}(s_0^{-1+(\mu_n-\nu)/m}) \quad \text{as} \quad s_0 \to 0 \tag{24}$$

with $-1 + (\mu_n - \nu)/m > 1$ for $n \geq 2$, showing the circle to be stable to all modes of perturbation, with the $n = 2$ mode decaying most slowly ($-1 + (\mu_n - \nu)/m$ is monotonically increasing in n).

For $m = 1$, δ vanishes, and the aspect ratio becomes

$$\frac{s(0,t)}{s(\pi/2,t)} \to 1 + 4\epsilon a_2 + \mathcal{O}(\epsilon^2) \quad \text{as} \quad s_0 \to 0$$

(agreeing with the result (A.9) found using the Baiocchi transform). Here the modes $n \geq 3$ are stable (since $\sigma_n = \mathcal{O}(s_0^{n-1}) = o(s_0)$)), whereas the $n = 2$ mode (associated with elliptic perturbations[4]) is neutrally stable (since $\sigma_2 = \mathcal{O}(s_0)$). Thus, if the perturbation is sufficiently symmetric (e.g., with n-fold symmetry for any $n = 3, 4, 5, \ldots$, leading to $a_2 = 0$) then $\sigma_2 = 0$ and the perturbations die out. However, in general, the bubble becomes elliptic in the limit, as explained in Appendix A; this neutral-stability property leads to subtleties in the asymptotic analysis that have been explored elsewhere (see [17, 32], for example).

Finally, for $m > 1$ we have $\delta > 0$, and the term

$$\frac{s_1(0,t) - s_1(\pi/2,t)}{s_0(t)}$$

blows up as $s_0 \to 0$. Here σ_n behaves as (24) with $-1+(\mu_n-\nu)/m < 1$ for $n < \sqrt{2m+2}$, so that the circle is unstable to modes with $n < \sqrt{2m+2}$, with the $n = 2$ mode growing the fastest. This result suggests that for $m > 1$ the bubble will, in general, stretch out in the extinction limit and we explore in sections 4-5 the generic ('thin-slit') asymptotic behaviour. Exceptions occur if the perturbation is suitably symmetric: if $a_2 = a_3 = \ldots = a_{n-1} = 0$ for some integer n, then the perturbations damp out provided $1 < m < \frac{1}{2}n^2 - 1$. Further, we conjecture that for $m > \frac{1}{2}n^2 - 1$, a solution with n-fold symmetry will evolve to an unstable similarity solution with n-fold symmetry. Such a solution is susceptible to weakly-nonlinear analysis in the limit $m \to (\frac{1}{2}n^2 - 1)^+$. These ideas are discussed further in section 6.

It is worth noting at this stage that the above classification already identifies the exceptional status of the Newtonian case $m = 1$ within this broader framework of power-law fluids.

[4] An ellipse, given by

$$\frac{x^2}{1+2\epsilon} + (1+2\epsilon)y^2 = 1,$$

can be written as $r = 1 + \epsilon \cos 2\theta + \mathcal{O}(\epsilon^2)$.

3.3. Transition timescale for the shear-thickening case $m > 1$

In the shear-thickening case the instability referred to above leads to nonlinear effects entering at leading order just before extinction. The correction term $\epsilon s_1(\theta, t)$ in the location of the free boundary becomes of the same order as $s_0(t)$ when $s_0 = \mathcal{O}(\epsilon^{1/\delta})$, implying that we need to rescale time according to

$$t = t_e + \epsilon^{\frac{1+m}{\delta m}} \hat{t}.$$

For the outer region for $\hat{t} = \mathcal{O}(1)$ we write (in order to match with the behaviour for $t_e - t = \mathcal{O}(1)$)

$$p \sim 1 + \epsilon^{\frac{m-1}{\delta}} \tilde{p}_1(r, \theta, \hat{t}),$$

wherein $\tilde{p}_1$ is the 'Green's function':

$$\boldsymbol{\nabla} \cdot \left(|\boldsymbol{\nabla} \tilde{p}_1|^{-(m-1)/m} \boldsymbol{\nabla} \tilde{p}_1 \right) = 0 \quad \text{in} \quad 0 < r < 1,$$

$$\tilde{p}_1 = 0 \quad \text{on} \quad r = 1, \quad \tilde{p}_1 \sim -\frac{a(\hat{t})}{r^{m-1}} \quad \text{as} \quad r \to 0$$

(cf. (6)-(7)), where $a(\hat{t})$ is some function to be determined by the boundary-value problem (25)-(27) below. Matching to (13) implies that $a(\hat{t})$ satisfies

$$a(\hat{t}) \sim \left[\frac{(1+m)(m-1)^{1/m}}{m} \right]^{\frac{m(m-1)}{1+m}} (-\hat{t})^{\frac{m(m-1)}{1+m}} \quad \text{as} \quad \hat{t} \to -\infty.$$

The inner scalings are

$$\hat{x} = \frac{x}{\epsilon^{1/\delta}}, \quad \hat{y} = \frac{y}{\epsilon^{1/\delta}}, \quad \hat{r} = \frac{r}{\epsilon^{1/\delta}},$$

and setting $p \sim \hat{p}_0(\hat{x}, \hat{y}, \hat{t})$ yields the moving-boundary problem

$$\hat{\boldsymbol{\nabla}} \cdot \left(|\hat{\boldsymbol{\nabla}} \hat{p}_0|^{-(m-1)/m} \hat{\boldsymbol{\nabla}} \hat{p}_0 \right) = 0 \quad \text{outside} \quad \partial\Omega, \tag{25}$$

$$\hat{p}_0 = 0, \quad \hat{V}_n = -|\hat{\boldsymbol{\nabla}} \hat{p}_0|^{(1-m)/m} \frac{\partial \hat{p}_0}{\partial \hat{n}} \quad \text{on} \quad \partial\Omega, \tag{26}$$

$$\hat{p}_0 \sim 1 - \frac{a(\hat{t})}{\hat{r}^{m-1}} \quad \text{as} \quad \hat{r} \to \infty, \tag{27}$$

where $\hat{\boldsymbol{\nabla}}$ is the scaled operator, $\hat{V}_n$ is the scaled normal velocity at the interface, and the (near-circular) initial data on $\partial\Omega$ are given by matching as $\hat{t} \to -\infty$.

The ultimate shape of a shrinking bubble in a near-circular Hele-Shaw cell for $m > 1$ is therefore dictated by solutions to the infinite-domain problem (25)-(27). Indeed, (25)-(27) could start as an infinite-domain problem for $m > 1$; for other m one might replace (27) by

$$\hat{p}_0 \sim \begin{cases} \hat{r}^{1-m} - a(\hat{t}) & \text{as} \quad \hat{r} \to \infty, \quad m < 1, \\ a(\hat{t}) \log \hat{r} + 1 & \text{as} \quad \hat{r} \to \infty, \quad m = 1. \end{cases} \tag{28}$$

Perturbing this about the radially symmetric solution, we find that the equivalent details to those presented in section 3.2 are identical. That is, the results of the stability analysis are, as is to be expected, equivalent to those of the finite-domain problem addressed above.

4. The long-thin Hele-Shaw cell

In this section we seek to shed further light on (1), (2) and (4) by considering the converse limit of a long, thin Hele-Shaw cell. For definiteness, we consider the illustrative case in which the Hele-Shaw cell boundary ∂B is the ellipse

$$\frac{x^2}{\alpha^2} + y^2 = 1, \tag{29}$$

and consider the limit $\alpha \to \infty$; it should be emphasised, however, that the most important implications of the results are of much broader relevance. We defer a discussion on these implications until section 5.

4.1. The Newtonian case, $m = 1$

From Appendix A.2, where a elliptical Hele-Shaw cell is treated for $m = 1$, the bubble's aspect ratio evolves from the value α at $t = 0$ to α^2 as $t \to t_e^-$, i.e. its aspect ratio becomes much larger than that of the domain itself when the domain is thin. The extinction time t_e has the limiting behaviour

$$t_e \sim \frac{1}{2} - \frac{1}{2\alpha^2} + \frac{1}{2\alpha^4} + \mathcal{O}(\alpha^{-6}) \quad \text{as} \quad \alpha \to \infty. \tag{30}$$

4.2. Perturbation analysis

As indicated previously, the Baiocchi approach does not apply in the more general case $m \neq 1$. Thus for $m \neq 1$ we begin by solving the problem (1), (2) and (4) (with ∂B given by the ellipse (29)) using a regular perturbation series with $\alpha \gg 1$.

Writing the bubble boundary $\partial\Omega$ as $y = s(x,t)$, we have to solve (in the first quadrant)

$$\boldsymbol{\nabla} \cdot \left(|\boldsymbol{\nabla} p|^{(1-m)/m} \boldsymbol{\nabla} p \right) = 0 \quad \text{in} \quad B \setminus \Omega(t), \tag{31}$$

$$p = 0, \quad \frac{\partial s}{\partial t} = -|\boldsymbol{\nabla} p|^{(1-m)/m} \left(\frac{\partial p}{\partial y} - \frac{\partial s}{\partial x}\frac{\partial p}{\partial x} \right) \quad \text{on} \quad y = s(x,t), \tag{32}$$

$$p = 1 \quad \text{on} \quad y = \sqrt{1 - \alpha^{-2}x^2}. \tag{33}$$

For $\alpha \gg 1$ we use the scaled variables

$$X = \frac{x}{\alpha}, \quad Y = y, \quad S(X,t) = s(\alpha X, t) \tag{34}$$

so the boundary ∂B takes the form $X^2 + Y^2 = 1$, and the interface is denoted by $Y = S(X,t)$. Introducing the expansions

$$p \sim P_0(X,Y,t) + \alpha^{-2} P_1(X,Y,t), \quad S \sim S_0(X,t) + \alpha^{-2} S_1(X,t), \tag{35}$$

we can easily obtain the leading solution

$$P_0 = \frac{Y - S_0(X,t)}{\sqrt{1-X^2} - S_0(X,t)} = 1 + \left(\frac{m}{1+m} \right)^{\frac{m}{1+m}} \frac{Y - \sqrt{1-X^2}}{t^{\frac{m}{1+m}}},$$

$$S_0 = \sqrt{1-X^2} - \left(\frac{1+m}{m}\right)^{\frac{m}{1+m}} t^{\frac{m}{1+m}}, \tag{36}$$

and the correction term to the interface is given by

$$S_1 = -\frac{m}{2(1+2m)}\left(\frac{1+m}{m}\right)^{\frac{2m}{1+m}} t^{\frac{2m}{1+m}} \frac{1}{(1-X^2)^{3/2}} - \frac{1}{2}\left(\frac{1+m}{m}\right)^{\frac{m}{1+m}} t^{\frac{m}{1+m}} \frac{X^2}{1-X^2};$$

certain further details are contained in Appendix C.

We denote the point in $X > 0$ at which the free boundary intersects the X-axis by $X = \Lambda(t)$, so that $S(\Lambda(t), t) = 0$. By setting $\Lambda \sim \Lambda_0(t) + \alpha^{-2}\Lambda_1(t)$, then

$$S_0 = 0, \quad \Lambda_1 \frac{\partial S_0}{\partial X} + S_1 = 0, \quad \text{on} \quad X = \Lambda_0,$$

which implies that

$$\Lambda_0 = \left[1 - \left(\frac{1+m}{m}\right)^{\frac{2m}{1+m}} t^{\frac{2m}{1+m}}\right]^{1/2}, \quad \Lambda_1 = -\frac{\frac{1+3m}{1+2m} - \left(\frac{1+m}{m}\right)^{\frac{2m}{1+m}} t^{\frac{2m}{1+m}}}{2\left[1 - \left(\frac{1+m}{m}\right)^{\frac{2m}{1+m}} t^{\frac{2m}{1+m}}\right]^{1/2}}. \tag{37}$$

Similarly, if the free boundary intersects the positive Y-axis at $Y = \Gamma(t)$, then $\Gamma(t) = S(0,t)$ and, setting $\Gamma \sim \Gamma_0(t) + \alpha^{-2}\Gamma_1(t)$, we find

$$\Gamma_0 = 1 - \left(\frac{1+m}{m}\right)^{\frac{m}{1+m}} t^{\frac{m}{1+m}}, \quad \Gamma_1 = -\frac{1+m}{2(1+2m)}\left(\frac{m}{1+m}\right)^{\frac{1-m}{1+m}} t^{\frac{2m}{1+m}}. \tag{38}$$

Using the intersection points above, the extinction time predicted on the basis of this analysis becomes

$$t_e \sim \frac{m}{1+m} - \frac{1}{\alpha^2}\frac{m}{2(1+2m)}. \tag{39}$$

For the Newtonian case this reduces to

$$t_e \sim \frac{1}{2} - \frac{1}{6\alpha^2},$$

the first correction term of which does *not* agree with (30). Consistent with this, we find as $t \to t_e^-$ that the aspect ratio of the bubble Λ/Γ blows up, regardless of the index m, which suggests we need to consider a further timescale.

According to the analysis given above, the interface advances in an essentially one-dimensional fashion in the y direction until very shortly before extinction. As illustrated in Figure 1(a), the 'outer' solutions suggest the free boundary contains a (near-2π angle) corner, this not in fact being the case; to provide a description of the inner regions one must first solve the Wiener-Hopf problem in Figure 1(b); this problem is likely to be tractable by the approach described in section 4.4.2 but we shall not pursue it here.

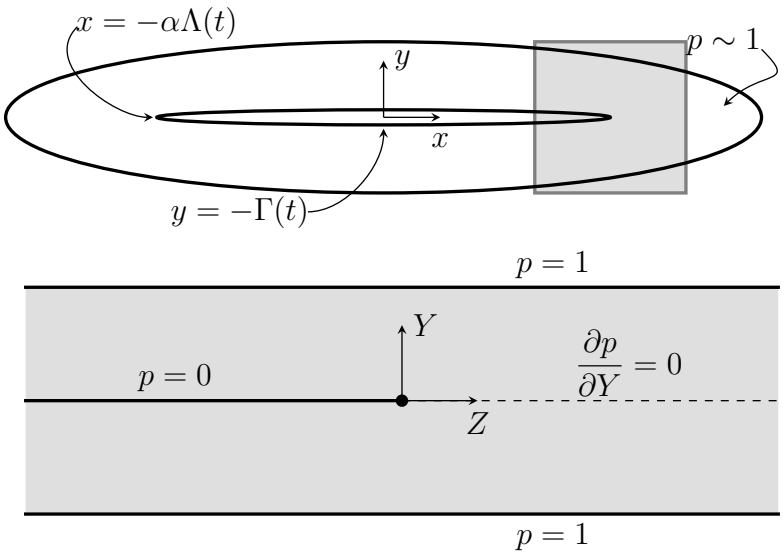

Figure 1. Top schematic: Slender-domain behaviour prior to near-extinction timescales. The limit problem corresponding to the shaded region is the 'slit-tip' Wiener-Hopf problem sketched in the bottom schematic. Here $X = \Lambda(t) + \alpha^{-2}Z$ with $Z = \mathcal{O}(1)$, $\Lambda(t)$ being determined by (37). There is a further (inner-inner) region about $(Z, Y) = (0, 0)$ wherein the solution is given by that in the appendix of [35].

4.3. Intermediate timescale

As extinction is approached the matching condition for the moving boundaries can be obtained from (36) and the leading order part of (39), namely

$$y = \pm S \sim t_e - t - \tfrac{1}{2}\alpha^{-2}x^2. \tag{40}$$

At this point it is worth mentioning that for a general long thin smooth geometry, taking the extinction point to be $\mathbf{x} = \mathbf{0}$, and rotating axes suitably, we can describe the moving boundaries by $y = S_\pm(x, t)$ in the upper and lower half-planes, respectively. In this case we have, as $t \to t_e^-$,

$$S_+(x,t) \sim q_e^+(t_e - t) - A_+\alpha^{-2}x^2, \quad S_-(x,t) \sim -q_e^-(t_e - t) + A_-\alpha^{-2}x^2,$$

where $q_e^+ = q_e^-$ for Dirichlet data and $A_+ = A_-$ in the symmetric case; these constants can be determined in terms of the fixed boundary locations.

Returning now to the long thin ellipse, from (40) we find the tips of the bubble have $x = \mathcal{O}(\alpha(t_e - t)^{1/2})$ and the rescalings on which the bubble length is comparable to the domain width (which is of order one) are

$$t = t_e + \alpha^{-2}\tilde{t}, \qquad \Lambda(t) = \alpha^{-1}\lambda(\tilde{t}), \quad \Gamma(t) = \alpha^{-2}\gamma(\tilde{t}). \tag{41}$$

A schematic of the behaviour on this time-scale is presented in Figure 2 (top). The subsequent evolution is determined by the Wiener-Hopf problem in Figure 2 (bottom); this has as the limit cases the other two with which we concern ourselves (i.e., the problems in Figure 1 (bottom) and Figure 3 (left)) and is thus the most challenging of the three; again, we shall not pursue it here but we note that its extinction behaviour

is determined by the analysis of section 4.4: this implies that the aspect ratio of the interface continues to increase in the shear-thickening case, so that the formulation in Figure 2 remains a valid description of the outer behaviour, whereas in the shear-thinning case it becomes small again (leading onto a final timescale in which the aspect ratio is $\mathcal{O}(1)$ and the interface finally evolves to a circle). For $m = 1$, the scalings in (41) correspond to the interface having aspect ratio $\mathcal{O}(\alpha^2)$, as required; in this case the aspect ratio associated with Figure 2 tends to a constant, corresponding to the interface being an ellipse with eccentricity near unity.

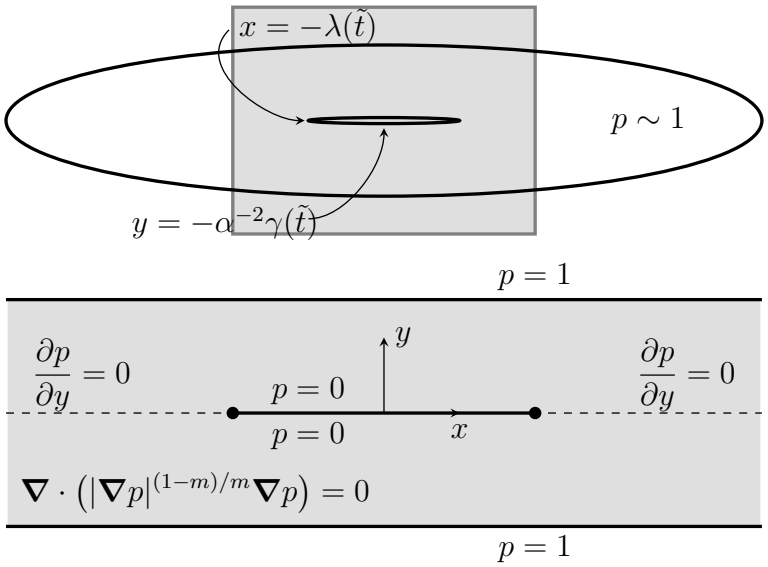

Figure 2. Top schematic: Slender-domain behaviour on the time-scale $t_e - t = \mathcal{O}(\alpha^{-2})$. Here the length of the bubble $2\lambda(\tilde{t}) = \mathcal{O}(1)$, while the width of the bubble $2\Gamma(t) = \mathcal{O}(\alpha^{-2})$. The shaded region corresponds to the near extinction Wiener-Hopf problem sketched in the bottom schematic.

Note that near extinction the behaviour away from the slit is determined as in section 2.2 (except that the formulation applies on an infinite strip instead of the finite domain B).

4.4. Near extinction behaviour

Here we consider the near extinction behaviour of the problem (31)-(33), the description being applicable to any long thin domain B for which there is only one extinction point.

4.4.1. Formulation As $t \to t_e^-$ there is an outer region away from the shrinking bubble, as detailed in section 2.2. To describe the inner region, we first observe the scalings (41) and write $s = \alpha^{-2}\tilde{s}(x, \tilde{t})$, so that the conditions on the bubble boundary linearise at leading order to

$$p = 0, \quad \frac{\partial \tilde{s}}{\partial \tilde{t}} = -\left(\frac{\partial p}{\partial y}\right)^{1/m} \quad \text{on} \quad y = 0, \quad 0 \leq x < \lambda(\tilde{t}).$$

Equation (1) subject to these boundary conditions has three scaling invariants (unlike the full moving-boundary problem, which (omitting boundary conditions on ∂B) has two, because s here need not scale in the same way as y), taking the subsequent analysis into the realms of second-kind self-similarity (cf. [13]). Using the similarity variables

$$\tilde{X} = \frac{x}{\lambda(\tilde{t})}, \quad \tilde{Y} = \frac{y}{\lambda(\tilde{t})},$$

where $\lambda(\tilde{t})$ will subsequently be determined by matching, the evolution of the bubble may be described by

$$\tilde{s} \sim \lambda^{\beta} F(\tilde{X}) \quad \text{as} \quad \tilde{t} \to 0^{-}, \tag{42}$$

provided that the pressure is of the form

$$p \sim \lambda^{1+m(\beta-1)} (-\dot{\lambda})^{m} \tilde{P}(\tilde{X}, \tilde{Y}) \quad \text{as} \quad \tilde{t} \to 0^{-},$$

where $\dot{\lambda} < 0$ and F satisfies the differential equation

$$\tilde{X} \frac{\mathrm{d}F}{\mathrm{d}\tilde{X}} - \beta F = - \left(\tilde{P}_{\tilde{Y}} \right)^{1/m} \Big|_{\tilde{Y}=0}, \tag{43}$$

β is a constant (dependent on m) to be found as part of the analysis, the dot denotes a derivative with respect to $\tilde{t}$, and the subscript $\tilde{Y}$ denotes a partial derivative. Thus β corresponds to a second-kind-similarity exponent and it is an appealing feature of the current problem that considerable analytical progress can be made towards its determination. The right-hand side of (43) depends on $\tilde{P}$, which is the solution to the Wiener-Hopf problem (corresponding to the walls in Figure 2 being scaled off to infinity - see also Figure 3)

$$\tilde{\boldsymbol{\nabla}} \cdot \left(\left| \tilde{\boldsymbol{\nabla}} \tilde{P} \right|^{(1-m)/m} \tilde{\boldsymbol{\nabla}} \tilde{P} \right) = 0 \quad \text{in} \quad \tilde{X} > 0, \quad \tilde{Y} > 0, \tag{44}$$

$$\text{on} \quad \tilde{X} = 0: \quad \frac{\partial \tilde{P}}{\partial \tilde{X}} = 0 \quad \text{for} \quad \tilde{Y} > 0, \tag{45}$$

$$\text{on} \quad \tilde{Y} = 0: \quad \tilde{P} = 0 \quad \text{for} \quad 0 < \tilde{X} < 1, \quad \frac{\partial \tilde{P}}{\partial \tilde{Y}} = 0 \quad \text{for} \quad \tilde{X} > 1, \tag{46}$$

$$\text{as} \quad \tilde{R} \to \infty: \quad \tilde{P} \sim \begin{cases} \tilde{A} \tilde{R}^{1-m} - \tilde{B} & m < 1 \\ \tilde{A} \log \tilde{R} - \tilde{B} & m = 1 \\ \tilde{A} - \tilde{B} \tilde{R}^{-(m-1)} & m > 1 \end{cases}, \tag{47}$$

where $\tilde{\boldsymbol{\nabla}}$ is the appropriately scaled operator, $\tilde{R} = (\tilde{X}^2 + \tilde{Y}^2)^{1/2}$, and $\tilde{A}$ and $\tilde{B}$ are constants. We also record the behaviour at the end of the slit, namely $\tilde{P} \sim \text{constant}\, \tilde{Y}$ as $\tilde{R} \to 0$. In order to specify a unique solution to (44)-(47)[5], we fix this constant to be unity, so that:

$$\text{as} \quad \tilde{R} \to 0: \quad \tilde{P} \sim \tilde{Y}. \tag{48}$$

[5] As it stands, (44)-(47) defines $\tilde{P}$ only up to an arbitrary multiple; we choose to remove this indeterminancy by prescribing the coefficient in (48) (i.e. as $\tilde{R} \to 0$) rather than in (47) (i.e. as $\tilde{R} \to \infty$) in order to facilitate the Wiener-Hopf analysis. Thus the values of $\tilde{A}$ and $\tilde{B}$ are both determined as part of the solution.

It should be emphasised that this problem determines for $m > 1$ the *generic* extinction behaviour, not just that for slender domains; we return to this point in section 5.

Once the solution for $\tilde{P}$ is calculated, the so-far unknown function $\lambda(t)$ can be determined as follows. For $m < 1$, matching with (10) (wherein A_e is determined as part of the solution to (8)-(9)) demands that

$$\lambda^{1+m(\beta-1)}(-\dot{\lambda})^m \tilde{A}\, \lambda^{-(1-m)} \sim A_e$$

so that

$$\lambda \sim (\beta+1)^{1/(\beta+1)} \left(A_e/\tilde{A}\right)^{1/m(\beta+1)} (-\tilde{t})^{1/(\beta+1)} \quad \text{as} \quad \tilde{t} \to 0^-. \tag{49}$$

For $m > 1$ we instead require, in view of (5) that

$$\lambda^{1+m(\beta-1)}(-\dot{\lambda})^m \tilde{A} \sim 1$$

so

$$\lambda \sim \left(\frac{m\beta+1}{\tilde{A}m}\right)^{1/(m\beta+1)} (-\tilde{t})^{1/(m\beta+1)} \quad \text{as} \quad \tilde{t} \to 0^-. \tag{50}$$

Moreover, we can then determine the behaviour of χ in (5) for $\tilde{t} = \mathcal{O}(1)$ by matching with (7) to give

$$\lambda^{1+m(\beta+1)}(-\dot{\lambda})^m \tilde{B}\, \lambda^{m-1} \sim \chi,$$

so that

$$\chi \sim \tilde{B}\, \lambda^{m\beta}(-\dot{\lambda})^m, \tag{51}$$

with λ given by (50).

It should be remarked that in the case of a slender domain, the problems (6)-(7) and (8)-(9) at leading order hold on an infinite strip, namely $-\infty < x < \infty$, $-1 < y < 1$ in the case in which the domain boundary is given by (29); in the outer regions, $X = \mathcal{O}(1)$ with $|X| > 0$, we have Φ in (6)-(7) and $1 - p_e$ in (8)-(9) being exponentially small in α, the JWKB ansatz

$$\Phi \sim e^{-\alpha\sigma(X)}\Theta(X, y),$$

yielding

$$\frac{\partial}{\partial y}\left(\left(\left(\frac{\partial\Theta}{\partial y}\right)^2 + \left(\frac{\mathrm{d}\sigma}{\mathrm{d}X}\right)^2\Theta^2\right)^{(1-m)/m}\frac{\partial\Theta}{\partial y}\right)$$
$$+\frac{1}{m}\left(\frac{\mathrm{d}\sigma}{\mathrm{d}X}\right)^2\left(\left(\frac{\partial\Theta}{\partial y}\right)^2 + \left(\frac{\mathrm{d}\sigma}{\mathrm{d}X}\right)^2\Theta^2\right)^{(1-m)/m}\Theta = 0$$

as the governing equation in an eigenvalue problem for $\mathrm{d}\sigma/\mathrm{d}X$.

4.4.2. Wiener-Hopf problem We reformulate (44)-(48) with the Legendre transform (with shifted origin of $\tilde{X}$)

$$\Psi = (\tilde{X}-1)\tilde{P}_{\tilde{X}} + \tilde{Y}\tilde{P}_{\tilde{Y}} - \tilde{P}, \quad \xi = \tilde{P}_{\tilde{X}}, \quad \eta = \tilde{P}_{\tilde{Y}}, \tag{52}$$

where we are now using subscripts to denote partial derivatives; the inverse transform reads

$$\tilde{P} = \xi\Psi_\xi + \eta\Psi_\eta - \Psi, \quad \tilde{X} = \Psi_\xi + 1, \quad \tilde{Y} = \Psi_\eta. \tag{53}$$

In the Legendre plane the governing equation

$$\left(\xi^2 + \frac{1}{m}\eta^2\right)\Psi_{\xi\xi} + \frac{2(m-1)}{m}\Psi_{\xi\eta} + \left(\frac{1}{m}\xi^2 + \eta^2\right)\Psi_{\eta\eta} = 0$$

is linear and, since the bubble boundary has been linearised to a fixed location (which in the current case implies that the transformed boundary conditions are also linear), we are therefore able to apply standard transform methods.

The problem in the Legendre plane is best suited to polar coordinates, and thus we define

$$\xi = -\rho\sin\phi, \quad \eta = \rho\cos\phi$$

(the nonstandard choice of $\phi = 0$ being made to allow a direct comparison with a similar problem considered by Amazigo [4]). In terms of these coordinates, the inner problem (44)-(46) transforms to

$$m\Psi_{\rho\rho} + \frac{1}{\rho}\Psi_\rho + \frac{1}{\rho^2}\Psi_{\phi\phi} = 0 \quad \text{in} \quad -\tfrac{1}{2}\pi < \phi < 0, \tag{54}$$

$$\text{on} \quad \phi = -\tfrac{1}{2}\pi: \quad \Psi_\phi = 0 \quad \text{for} \quad \rho > 0, \tag{55}$$

$$\text{on} \quad \phi = 0: \quad \Psi_\phi = \rho \quad \text{for} \quad 0 < \rho < 1, \quad \Psi = 0 \quad \text{for} \quad \rho > 1, \tag{56}$$

$$\text{as} \quad \rho \to 0: \quad \Psi \sim \begin{cases} \text{constant}\,\rho^{-(1-m)/m} + \text{constant} - \xi, & m < 1, \\ \text{constant}\,\log\rho + \text{constant} - \xi, & m = 1, \\ \text{constant} + \text{constant}\,\rho^{(m-1)/m} - \xi, & m > 1, \end{cases} \tag{57}$$

$$\text{as} \quad \rho \to \infty: \quad \Psi \sim \text{constant}\,\rho^{-1/m}\sin\phi. \tag{58}$$

To apply the Wiener-Hopf technique, we also require the limiting behaviour:

$$\text{as} \quad \rho \to 1^-: \quad \Psi(\rho, 0) \sim \text{constant}\,(1-\rho)^{3/2}, \tag{59}$$

$$\text{as} \quad \rho \to 1^+: \quad \Psi_\phi(\rho, 0) \sim 1 + \text{constant}\,(\rho-1)^{1/2}. \tag{60}$$

The conditions (57)-(60) are found by separating variables in the appropriate limit; the constant must be determined as part of the solution. A schematic of the Legendre transform plane is given in Figure 3.

We solve (54)-(58) below with the use of a Mellin transform and the Wiener-Hopf technique. As mentioned above, this problem is similar to one solved by Amazigo [4] (see [5], [12] for other variations), who considered a crack in a power-law (work-hardening) solid under anti-plane shear (longitudinal shear). In that context the particular value

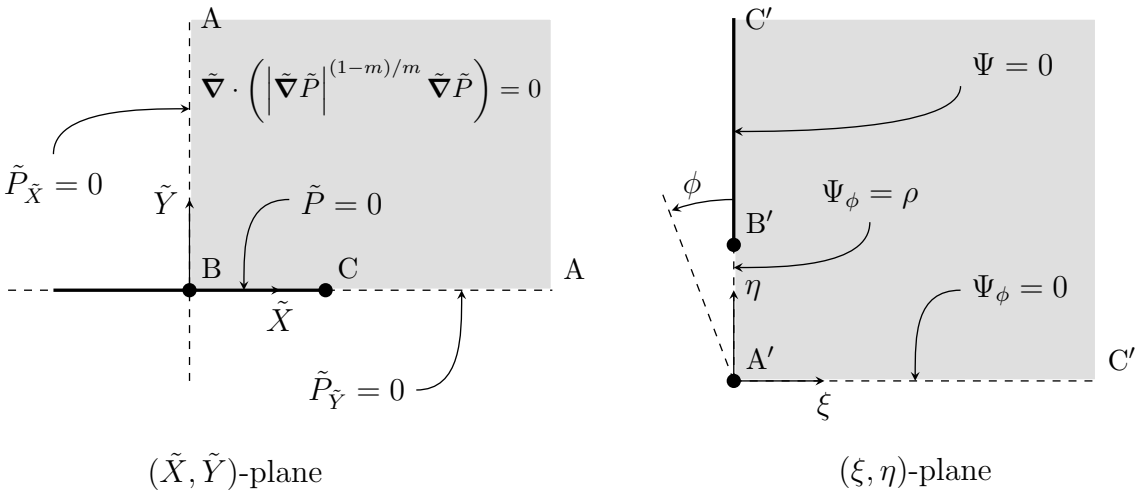

Figure 3. Mapping from the physical plane to the Legendre plane (A maps to A′, and so on).

$m = 1$ corresponds to a Hookean elastic material. Amazigo [4] considers (54)-(56), (58), but instead of (57) he has Ψ bounded as $\rho \to 0$, and instead of (59)-(60) he has

$$\text{as} \quad \rho \to 1^- : \quad \Psi(\rho, 0) \sim \text{constant}\, (1-\rho)^{1/2}, \tag{61}$$

$$\text{as} \quad \rho \to 1^+ : \quad \Psi(\rho, 0) \sim \text{constant}\, (\rho-1)^{-1/2}. \tag{62}$$

Much of our working follows [4], and we try to use the same notation where possible.

We apply the Mellin transform, defined by

$$\bar{\Psi}(s, \phi) = \int_0^\infty \Psi(\rho, \phi) \rho^{s-1} \, \mathrm{d}\rho, \tag{63}$$

to (54), and note that, given the two limits (57)-(58), we can conclude that this definition holds in the vertical strip $\max(1/m - 1, 0) < \mathrm{Re}(s) < 1/m$. Adopting the same notation as [4], we define the functions $u(\rho)$ and $g(\rho)$ by

$$u(\rho) = \begin{cases} 0, & 0 < \rho < 1, \\ \Psi_\phi(\rho, 0), & \rho > 1 \end{cases}, \quad g(\rho) = \begin{cases} \Psi(\rho, 0), & 0 < \rho < 1, \\ 0, & \rho > 1 \end{cases},$$

and note that since $u(\rho) = 0$ for $0 < \rho < 1$ and $g(\rho) = 0$ for $\rho > 1$, the transformed functions $\bar{u}_-(s)$ and $\bar{g}_+(s)$ are analytic in the left-half plane $\mathrm{Re}(s) < 1/m$ and the (overlapping) right-half plane $\mathrm{Re}(s) > \max(1/m - 1, 0)$, respectively.

Applying the Mellin transform (63) to (54)-(55) gives

$$\bar{\Psi}_{\phi\phi} + \omega^2(s) \bar{\Psi} = 0 \quad \text{in} \quad \max(1/m - 1, 0) < \mathrm{Re}(s) < 1/m,$$

$$\bar{\Psi}_\phi = 0 \quad \text{on} \quad \phi = -\tfrac{1}{2}\pi,$$

$$\bar{\Psi}_\phi = \frac{1}{1+s} + \bar{u}_-(s), \quad \bar{\Psi} = \bar{g}_+(s) \quad \text{on} \quad \phi = 0,$$

where $\omega^2(s) \equiv s[m(s+1) - 1]$, whose solution leads to

$$\bar{g}_+(s) = -\left[\frac{1}{1+s} + \bar{u}_-(s) \right] q(s) \ \text{ in } \ \max(1/m - 1, 0) < \mathrm{Re}(s) < 1/m, \tag{64}$$

$$q(s) \ \equiv \omega^{-1}(s) \cot\left[\tfrac{1}{2} \pi \omega(s) \right] \tag{65}$$

(the label p is used in [4] instead of q). To solve the Wiener-Hopf type equation (64) we first write

$$q(s) = \frac{N_-(s)}{D_+(s)}, \tag{66}$$

where $N_-(s)$ is analytic and non-zero in the left-half plane $\mathrm{Re}(s) < 1/m$ and $D_+(s)$ is analytic and non-zero in the right-half plane $\mathrm{Re}(s) > \max(1/m - 1, 0)$ (see (68)-(69) for the precise forms for $N_-(s)$ and $D_+(s)$). Thus we have

$$-\bar{g}_+(s)D_+(s) = \left[\left(\frac{1}{1+s}\right)_+ + \bar{u}_-(s)\right] N_-(s)$$

in $\max(1/m - 1, 0) < \mathrm{Re}(s) < 1/m$, where the subscript $+$ is again used to denote a function analytic in $\mathrm{Re}(s) > \max(1/m - 1, 0)$. After noting that $1/(1 + s)$ has a simple pole at $s = -1$ (which lies in the left-half plane $\mathrm{Re}(s) < 1/m$), we apply the decomposition

$$\frac{N_-(s)}{1+s} = J_-(s) + J_+(s),$$

where

$$J_-(s) = \frac{N_-(s) - N_-(-1)}{1+s}, \quad J_+(s) = \frac{N_-(-1)}{1+s}.$$

This has the effect of removing the singularity at $s = -1$ from $N_-/(1+s)$, so that $J_-(s)$ and $J_+(s)$ are analytic in $\mathrm{Re}(s) < 1/m$ and $\mathrm{Re}(s) > \max(1/m - 1, 0)$, respectively. It follows that

$$J_-(s) + \bar{u}_-(s)N_-(s) = -\bar{g}_+(s)D_+(s) - J_+(s) \tag{67}$$

in $\max(1/m - 1, 0) < \mathrm{Re}(s) < 1/m$. The standard Wiener-Hopf argument is that, since the left-hand side of (67) is analytic in $\mathrm{Re}(s) < 1/m$ and the right-hand side is analytic in $\mathrm{Re}(s) > \max(1/m - 1, 0)$, by analytic continuation both sides define an analytic function in the entire s-plane.

We now seek to determine the behaviour of each side of (67) in the far-field. A satisfactory factorisation of the function $q(s)$ in the form (66) is given by Amazigo [4], namely

$$N_-(s) = 2^{-\sqrt{m}s} \frac{\prod_{k=1}^{\infty} \left(\gamma_{2k-1}^+ - a_{2k-1}s\right) e^{a_{2k-1}\bar{s}}}{\prod_{k=1}^{\infty} \left(\gamma_{2k}^+ - a_{2k}s\right) e^{a_{2k}\bar{s}}}, \tag{68}$$

$$D_+(s) = m\pi 2^{-\sqrt{m}s-1} s \left(s + 1 - \frac{1}{m}\right) \frac{\prod_{k=1}^{\infty} \left(\gamma_{2k}^- - a_{2k}s\right) e^{-a_{2k}\bar{s}}}{\prod_{k=1}^{\infty} \left(\gamma_{2k-1}^- - a_{2k-1}s\right) e^{-a_{2k-1}\bar{s}}}, \tag{69}$$

with (in the notation of [4] rather than that of section 3)

$$a_n = \frac{m^{1/2}}{n}, \ \gamma_n^{\pm} = \frac{1 - m \pm \left((m-1)^2 + 4n^2m\right)^{1/2}}{2nm^{1/2}}, \ \bar{s} = s + \frac{m-1}{2m}. \tag{70}$$

The far field behaviour of $N_-(s)$ as $s \to \infty$ is ([4])

$$N_-(s) \sim \left(\tfrac{1}{2}\pi\right)^{1/2} m^{1/4} 2^{(m-1)/2\sqrt{m}} (-s)^{1/2} \quad \mathrm{Re}(s) < 1/m. \tag{71}$$

The limiting form for $\bar{u}_-(s)$ is determined with the use of (60). After integrating by parts once and then applying Watson's lemma, we find that

$$\bar{u}_-(s) = \int_{-\infty}^{0} u\left(e^{-x}\right) e^{-sx}\,\mathrm{d}x \sim -\frac{1}{s} + \frac{\text{constant}}{(-s)^{3/2}} \quad \text{as} \quad |s| \to \infty \tag{72}$$

for $\mathrm{Re}(s) < 1/m$. It follows that the left-hand side of (67) vanishes in the limit $|s| \to \infty$, $\mathrm{Re}(s) < 1/m$ (and with the use of (59) a similar argument can be applied to show that the right-hand side (67) vanishes in the right-hand plane), thus by Liouville's theorem the analytic function defined by each side of (67) must be identically zero. (We note that in Amazigo [4], the conditions (61)-(62) do *not* lead to both sides of (67) vanishing in the far field; instead, they approach a constant that must be determined by imposing the condition that Ψ be bounded as $\rho \to 0$. In that respect our problem is slightly less challenging than that solved in [4].)

For our purposes it suffices to calculate $u(\rho)$. After rearranging the right-hand side of (67) (which is identically zero), we find

$$\bar{u}_-(s) = \frac{1}{1+s}\left(\frac{N_-(-1)}{N_-(s)} - 1\right), \tag{73}$$

thus, by inverting the Mellin transform in (73),

$$u(\rho) = \frac{1}{2\pi i}\int_{c-i\infty}^{c+i\infty} \frac{1}{1+s}\left(\frac{N_-(-1)}{N_-(s)} - 1\right)\rho^{-s}\,\mathrm{d}s, \tag{74}$$

where $\max(1/m - 1, 0) < c < 1/m$. For $\rho > 1$ we close the contour with a large semi-circle in the right-hand plane. The only singularities inside the contour are due to the zeros of $N_-(s)$ which, by observing the form of $N_-(s)$ given in (68), are seen to occur at $s = \gamma_{2n-1}^+/a_{2n-1} = C_n$ for $n = 1, 2, \ldots$. The residue of $1/N_-(s)$ at $s = C_n$ is

$$-\frac{2^{m^{1/2}C_n}\prod_{k=1}^{\infty}\left(\gamma_{2k}^+ - a_{2k}C_n\right)e^{a_{2k}\bar{C}_n}}{a_{2n-1}e^{a_{2n-1}\bar{C}_n}\prod_{k=1\,(k\neq n)}^{\infty}\left(\gamma_{2k-1}^+ - a_{2k-1}C_n\right)e^{a_{2k-1}\bar{C}_n}},$$

where

$$\bar{C}_n = C_n + \frac{m-1}{2m}.$$

Thus for $\rho > 1$,

$$u(\rho) = \sum_{n=1}^{\infty}\left\{\frac{2^{m^{1/2}C_n}N_-(-1)\prod_{k=1}^{\infty}\left(\gamma_{2k}^+ - a_{2k}C_n\right)e^{a_{2k}\bar{C}_n}}{a_{2n-1}e^{a_{2n-1}\bar{C}_n}(1+C_n)\prod_{k=1\,(k\neq n)}^{\infty}\left(\gamma_{2k-1}^+ - a_{2k-1}C_n\right)e^{a_{2k-1}\bar{C}_n}}\right\}\rho^{-C_n} \tag{75}$$

where we recall that $N_-(s)$, a_n, γ_n^+ are defined in (68) and (70). On the slit we have $\tilde{X} = 1 - u(\rho)/\rho$, and thus from $(52)_3$ we can compute $\tilde{P}_{\tilde{Y}}$ implicitly as a function of $\tilde{X}$. This function provides the right-hand side of (43), so we can now solve for $F(\tilde{X})$, the shape of the bubble near extinction; this calculation is included below in section 4.4.3.

For the Newtonian case $m = 1$, we have the simplifications $C_n = 2n - 1$, $\gamma_n^{\pm} = \pm 1$, $a_n = 1/n$. After applying the relevant identities for Gamma functions (including Euler's infinite product definition and the reflection formula [1]), we find $N_-(-1) = \pi/2$ and

$$u(\rho) = \sum_{n=1}^{\infty}\left\{\frac{2^{1-2n}(2n-2)!}{n((n-1)!)^2}\right\}\rho^{1-2n}, \quad m = 1,$$

so that on the slit

$$\tilde{X} = 1 - \sum_{n=1}^{\infty} \left\{ \frac{2^{1-2n}(2n-2)!}{n((n-1)!)^2} \right\} \left(\tilde{P}_{\tilde{Y}} \right)^{-2n}. \tag{76}$$

Further manipulation using the duplication formula for Gamma functions ([1]) gives

$$\tilde{X} = \sum_{n=1}^{\infty} \left\{ \frac{\sqrt{\pi}}{n!(1-2n)\Gamma(\frac{1}{2}-n)} \right\} \left(\tilde{P}_{\tilde{Y}} \right)^{-2n}. \tag{77}$$

The solution in the physical plane for $m = 1$ is simply

$$\tilde{P} = \tilde{\mu}, \quad \tilde{P}_{\tilde{Y}} = \frac{\cosh\tilde{\mu}\sin\tilde{\nu}}{\sin^2\tilde{\nu} + \sinh^2\tilde{\mu}},$$

where $\tilde{\mu}$ and $\tilde{\nu}$ are elliptic coordinates defined by

$$\tilde{X} = \cosh\tilde{\mu}\cos\tilde{\nu}, \quad \tilde{Y} = \sinh\tilde{\mu}\sin\tilde{\nu}.$$

On the slit $\tilde{\mu} = 0$, so that for $0 < \tilde{X} < 1$, $\tilde{Y} = 0$,

$$\tilde{P}_{\tilde{Y}} = \left(1 - \tilde{X}^2\right)^{-1/2} \quad \text{or} \quad \tilde{X} = \left(1 - (\tilde{P}_{\tilde{Y}})^{-2}\right)^{1/2}. \tag{78}$$

Expanding the latter expression about $\tilde{P}_{\tilde{Y}} = \infty$ using the binomial theorem gives the series solution (77), as required.

4.4.3. Evolution of the shrinking bubble Recall that the bubble shape near extinction is given by (42), where F is determined by (43). In terms of the Legendre variables, this differential equations is

$$\frac{\mathrm{d}F}{\mathrm{d}\eta} - \beta \left(\frac{\Psi_{\xi\eta}}{\Psi_\xi + 1} \right) F = -\left(\frac{\Psi_{\xi\eta}}{\Psi_\xi + 1} \right) \eta^{1/m} \quad \text{for} \quad \xi = 0, \quad \eta > 1, \tag{79}$$

with the boundary conditions that

$$\frac{1}{\Psi_{\xi\eta}} \frac{\mathrm{d}F}{\mathrm{d}\eta} = 0 \quad \text{on} \quad \eta = 1, \quad F = 0 \quad \text{as} \quad \eta \to \infty \tag{80}$$

(two conditions are required on the first-order equation (79) to determine the value of β).

Now, from (71) and (73) we can determine the constant in (72), and thus derive the result

$$u(\rho) \sim 1 - \frac{2^{1+1/2m} N_-(-1)}{\pi m^{1/4}} (\rho - 1)^{1/2} + (\rho - 1) + \mathcal{O}((\rho - 1)^{3/2})$$

as $\rho \to 1^+$, which in turn implies that

$$\tilde{X} \sim \frac{2^{(1+2m)/(2m)} N_-(-1)}{\pi m^{1/4}} (\rho - 1)^{1/2} + \mathcal{O}((\rho - 1)^{3/2}) \quad \text{as} \quad \rho \to 1^+.$$

Using this information and the original differential equation (43), we now find

$$F \sim \frac{1}{\beta} - \frac{\pi^2}{2^{2+1/m}(2-\beta)m^{1/2}N_-(-1)^2} \tilde{X}^2 + \mathcal{O}(\tilde{X}^4) \quad \text{as} \quad \tilde{X} \to 0^+, \tag{81}$$

provided $\beta \neq 2$. With this behaviour we can now write the solution to (43) that satisfies the first of (80) as

$$F = \frac{1}{\beta}\eta^{1/m} - \frac{1}{m\beta}(\Psi_\xi + 1)^\beta \int_1^\eta (\Psi_\xi + 1)^{-\beta}\eta^{1/m-1}\,\mathrm{d}\eta,$$

where, again, Ψ_ξ is evaluated at $\xi = 0$. In order to satisfy the second condition in (80), we choose the appropriate value of β (for each value of m) by solving the algebraic equation

$$\lim_{\eta\to\infty}\left(\frac{1}{\beta}\eta^{1/m} - \frac{1}{m\beta}(\Psi_\xi + 1)^\beta \int_1^\eta (\Psi_\xi + 1)^{-\beta}\eta^{1/m-1}\,\mathrm{d}\eta\right) = 0\,;$$

this task must be undertaken numerically. Thus, given that for $\xi = 0$ we have $\Psi_\xi = -u(\eta)/\eta$, where $u(\rho)$ is given by the infinite series (75), we can compute the parametric solution

$$\left.\begin{aligned} \tilde{X} &= 1 - \frac{u(\eta)}{\eta}, \\ F &= \frac{1}{\beta}\eta^{1/m} - \frac{1}{m\beta}\left(1 - \frac{u(\eta)}{\eta}\right)^\beta \int_1^\eta \left(1 - \frac{u(\eta)}{\eta}\right)^{-\beta} \eta^{1/m-1}\,\mathrm{d}\eta \end{aligned}\right\} \text{for } \eta > 1.$$

Note that for a Newtonian fluid with $m = 1$, the parametric solution reduces to

$$F(\tilde{X}) = \sqrt{1 - \tilde{X}^2}. \tag{82}$$

In this case the bubble shape and pressure field are described by

$$\tilde{s} \sim \lambda F(\tilde{X}), \quad p \sim \lambda\dot{\lambda}\tilde{P}(\tilde{X}, \tilde{Y}) \quad \text{as} \quad \tilde{t} \to 0^-.$$

Representative examples of the shape of $F(\tilde{X})$ are included in Figure 4, where it should be remembered that in original variables $F(\tilde{X}) = \alpha^2 s(x,t)/\lambda(t)$ and $\tilde{X} = x/\lambda(t)$. These are calculated using the parametric solution above. (As a check on the calculation, we also numerically evaluated the alternative integral solution

$$F = \tilde{X}^\beta \int_{\tilde{X}}^1 \tilde{X}^{-1-\beta}\eta^{1/m}\,\mathrm{d}\tilde{X},$$

which identically satisfies $F(1) = 0$, a condition that is equivalent to the second of (80).) For $m = 1$ these curves are ellipses, while for $m \neq 1$ the shapes can be thought of as generalised ellipses: they are parameter-free shapes that have ellipses (rescaled on the unit circle) as special cases. The numerical results strongly suggest that $\beta \to 2^-$ as $m \to \infty$, implying that $F(0) \to 1/2^+$ in the limit; this is consistent with (81), which for $\beta > 2$ would give $F''(0) > 0$, which is not allowed. In the converse limit $m \to 0$, we conjecture that $\beta \to 0^-$ and $F(0) \to \infty$.

Of interest is the aspect ratio of the shrinking bubble, which in physical coordinates becomes

$$\frac{\lambda}{\Gamma} = \frac{\lambda}{\alpha^{-2}\lambda^\beta F(0)} = \alpha^2\beta\lambda^{1-\beta}, \tag{83}$$

where we recall that $\lambda(t)$ represents the x-coordinate of the bubble tip, while $\Gamma(t)$ is the y-coordinate at $x = 0$. In the limit $\lambda \to 0^+$, this quantity crucially depends on

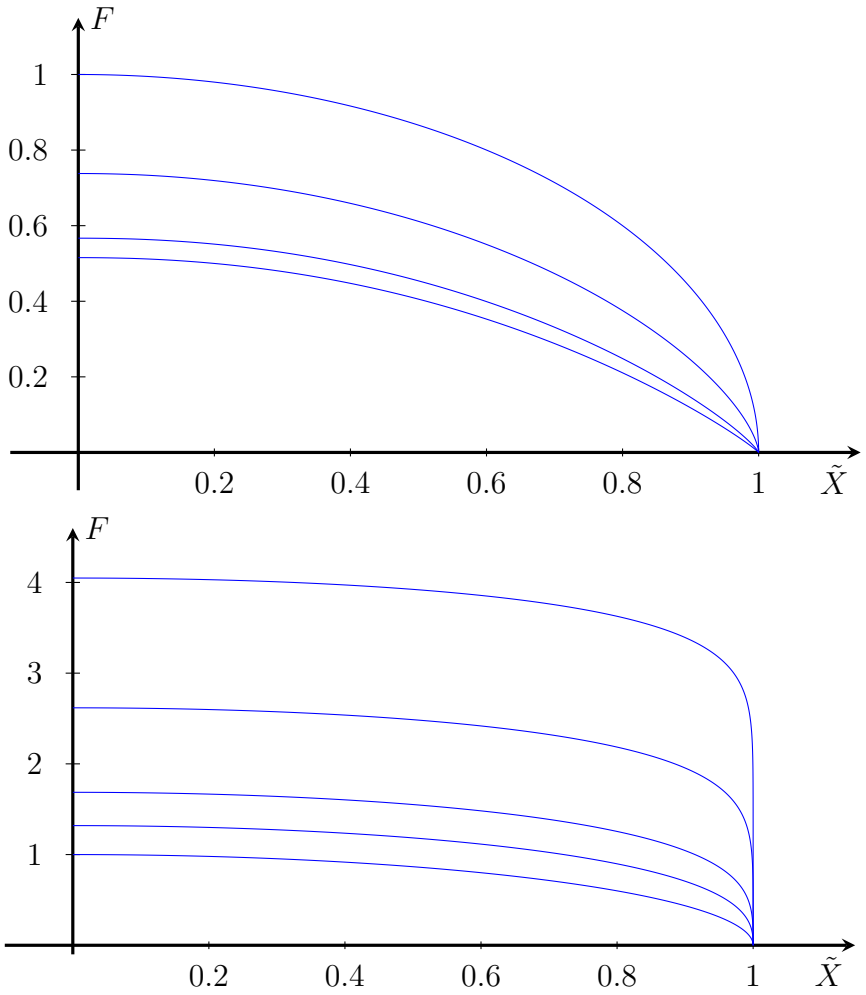

Figure 4. Plots of the function $F(\tilde{X})$ versus $\tilde{X}$. In part (a), from top to bottom, profiles are for $m = 1$ ($\beta = 1$), 2 (1.355), 5 (1.764) and 10 (1.940). In part (b), top to bottom, $m = 0.1$ ($\beta = 0.247$), 0.2 (0.382), 0.4 (0.593), 0.6 (0.758) and 1 (1).

the exponent $1 - \beta$, whose relationship to m is illustrated in Figure 5. We see that for a shear-thickening fluid ($m > 1$), the aspect ratio of the bubble increases indefinitely as $\lambda \to 0^+$. On the other hand, for shear-thinning fluids ($m < 1$), the aspect ratio grows without bound for the long thin limit $\alpha \to \infty$ (with λ fixed), but shrinks as λ decreases (with α fixed). Thus for $m < 1$ a further time-scale must be treated, when $\lambda = \mathcal{O}(\alpha^{-2/(1-\beta)})$, on which the aspect ratio of the bubble is of order one, and the infinite domain problem describes the inner solution. This is analogous to the transition timescale discussed for the converse case in section 3.3 and we do not elaborate on it further. Since $\beta = 1$ for $m = 1$, the Newtonian case is again identified as the borderline case for which the aspect ratio (83) neither grows nor shrinks.

The asymptotic behaviour

$$F \sim \frac{(1+m)\mathcal{K}^{1/(1+m)}}{m}(1-\tilde{X})^{m/(1+m)} \quad \text{as} \quad \tilde{X} \to 1^- \tag{84}$$

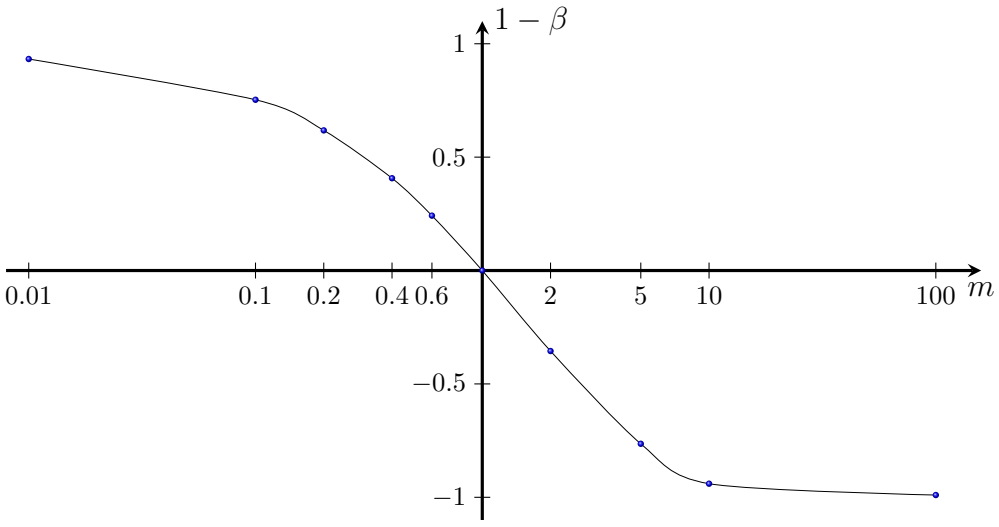

Figure 5. Numerically calculated values of $1-\beta$ versus m.

applies at the tip of the bubble, where

$$\mathcal{K} = \frac{2^{m^{-1/2}} m^{1/2} N_-(-1) \prod_{k=1}^{\infty} \left(\gamma_{2k}^{+} - a_{2k}/m\right) e^{a_{2k}(m+1)/2m}}{(1+m)e^{(m+1)/2m^{1/2}} \prod_{k=2}^{\infty} \left(\gamma_{2k-1}^{+} - a_{2k-1}/m\right) e^{a_{2k-1}(m+1)/2m}}.$$

Here $\mathcal{K}$ is the constant in the curly brackets in (75) with the dummy variable n set to unity; it reduces to $\mathcal{K} = 1/2$ for the borderline case $m = 1$. The solution (84) matches with the far-field solutions of the explicit travelling-wave solutions of the appendix of [35], which (as above) provide the (fully two-dimensional) inner behaviour at the tips of the contracting bubbles. By noting that

$$\frac{(1+m)\mathcal{K}^{1/(1+m)}}{m}(1-\tilde{X})^{m/(1+m)} \sim \mathcal{K}\left(\frac{1+m}{m}\right)\left(\frac{-\tilde{X}}{\mathcal{K}}\right)^{m/(1+m)}$$

as $\tilde{X} \to -\infty$, we can compare directly with [35], giving $C = \mathcal{K}/m$ as the value of the constant in equation (A6) therein.

5. The Hele-Shaw cell of order one aspect ratio

Having deliberately explored in sections 3 and 4 limit problems that lead naturally to the two extremes of extinction behaviour (that is, near-circular domains leading ultimately to a circular interface when $m < 1$ and thin domains leading to a slit-like interface whose aspect ratio grows without bound when $m > 1$), our discussion of the general case can be brief because these extremes of behaviour appear to be generic.

For $m < 1$ we believe that the extinction behaviour always involves the interface becoming circular in the limit (the details of ∂B are irrelevant in the limit and the radially symmetric solution to the infinite-domain problem is stable; for a thin domain, the aspect ratio of the bubble initially increases significantly but for $m < 1$ it flattens up again as it approaches extinction).

For $m > 1$ the generic extinction behaviour is of slit type and is described by exactly the Wiener-Hopf problem (44)-(47) (and the associated anomalous exponent β) summarised in Figure 3 (left), for which the details of ∂B are again of no importance. The sole significant difference from the discussion of section 4.4.1 is that Φ is determined from the full problem (6)-(7), not from its infinite-strip limit; the time dependence can still be inferred from (50) and (51) on taking $\alpha = \mathcal{O}(1)$ in the relevant scalings. In addition, for $m > 1$ a series of secondary bifurcations is present that lead (as m passes through $\frac{1}{2}n^2 - 1$ for $n = 3, 4, \ldots$) to a sequence of unstable self-similar solutions having 3,4,... (discrete) rotation symmetries (akin to n-sided 'polygonial' bubbles with rounded corners; these solutions will be realised for initial boundary value problem having the requisite symmetry, and can occur non-generically in other cases). To illustrate the role of such solutions, we note that the four-fold-symmetric ones that exist for $m > 7$ can be expected to result within the class of domains that are symmetric about both x and y axes, for those domains on the borderline between those in which the slit is aligned along the x axis and those in which it is aligned along the y axis (for $1 < m < 7$ the limit shape in this borderline case can instead be expected to be circular). The primary bifurcation at $m = 1$ to ellipses is of an exceptional form (see [29]) due to the special properites of the classical Hele-Shaw problem; the subsequent bifurcations are not expected to be, though a weakly nonlinear analysis would be worth pursuing, in particular in order to confirm whether or not they are supercritical.

6. Discussion

Using the linear stability analysis of section 3, it is easy to show that, on the bubble boundary, the shear rate $\|\mathbf{D}\|$ becomes unbounded as $s_0 \to 0$ regardless of the index m. The viscosity μ accordingly vanishes as $s_0 \to 0$ for $m < 1$ and blows up as $s_0 \to 0$ for $m > 1$. The physical interpretation of the unstable radially extinction behaviour in the shear-thickening case $m > 1$ is that as the bubble contracts the viscosity increases, making it more and more difficult for the fluid to flow, in effect meaning that an increasingly thin bubble shape can get 'locked in'; conversely in the shear-thinning case $m < 1$ the fluid can readily flow to attain the symmetric state.

The behaviour in the shear-thickening case, including the self-similar solutions noted towards the end of section 3.2 (and again in section 5) is analogous to that of the focusing problem (3) for the porous medium equation (see [8, 9, 10, 14]). In that context the $\gamma = \infty$ case (which coincides with present contracting bubble problem with $m = 1$) is neutrally stable, but as γ decreases there exists an increasing number of non-radial (unstable) solutions with n-fold symmetry, in addition to the stable 'slit' solutions. The limit $\gamma = 0$ yields the eikonal equation

$$\frac{\partial v}{\partial t} = |\boldsymbol{\nabla} v|^2$$

(obtained by setting $v = u^\gamma/\gamma$ in (3) and taking the limit $\gamma \to 0$), for which there are infinitely many unstable modes [7].

Self-similar solutions to the infinite-domain problem (1), (2) and (27) or (28) of course satisfy a quasi-steady free boundary problem. For the Newtonian case $m = 1$ it is known that the complement of Ω is a null quadrature domain, and the only possibility is then that ∂B be an ellipse (for details of these results, generalisations to $\mathbb{R}^3$, and relationships to the gravitational potential, see [16, 17, 18, 25, 26], for example). Since the Hele-Shaw problem is time-reversible, the linear-stability results for the infinite-domain problem (mentioned at the end of section 3.3) are reversed for growing bubbles (note that the bubble growth problem is well known to be ill-posed). The (highly unstable) bubble shapes that can grow to infinity, clearing away all the fluid, can be thought of as 'null quadrature domains' for the p-Laplacian, as in [29], and those constructed by the Wiener-Hopf method in section 4.4 for $m < 1$ are plausible candidates, since in the shear-thinning case they become longer and thinner as they grow.

A relevant generalisation of the focusing problem discussed in section 1 comes from treating the doubly nonlinear diffusion equation with appropriate boundary conditions, namely

$$\frac{\partial u}{\partial t} = \boldsymbol{\nabla} \cdot \left(u^\gamma |\boldsymbol{\nabla} u|^{(1-m)/m} \boldsymbol{\nabla} u \right), \quad u = u^\gamma |\boldsymbol{\nabla} u|^{(1-m)/m} \frac{\partial u}{\partial n} = 0 \text{ on } \partial\Omega, \tag{85}$$

as the governing equation. Setting $m = 1$ in (85) recovers the focusing problem for the porous medium equation (3), while the limit $\gamma = \infty$ in (85) can lead to the Hele-Shaw problem for a power-law fluid (the problem considered in this paper). The generalised focusing problem (85) is considered briefly by Gil & Vázquez [20], but only in the radially symmetric case. An interesting problem would be to investigate what happens when this symmetry is broken: at least for m slightly less than unity, it is plausible that there exists a finite value of γ at which the extinction behaviour exhibits a transition from slits to circles.

We conclude by briefly noting related problems that may be worth pursuing. These include the analogous higher dimensional problems and asymptotic investigations of the extinction in the limits. For example, a difference worth highlighting when the dimension $N = 3$ is that (11) switches behaviour at $m = 1/2$ rather than at the Newtonian value $m = 1$, which is likely to have implications for the extinction behaviour; we leave the analysis of this case as a worthwhile open problem. Nevertheless, we note that a stability analysis analogous to section 3, using spherical polar coordinates (r, θ, ϕ) instead of cylindrical polars (r, θ), leads to (in the obvious notation)

$$s_1(\theta, \phi) = \sum_{n=2}^{\infty} \sum_{k=0}^{n} \sigma_{nk}(t) Y_n^k(\theta, \phi),$$

where the Y_n^k are the usual spherical harmonics, with

$$\sigma_{nk} = \mathcal{O}(s_0^{-2+(\mu_n - \nu)/m}) \quad \text{as} \quad s_0 \to 0$$

(cf. (24)) and

$$\nu = \tfrac{1}{2} - m, \quad \mu_n = \tfrac{1}{2}\sqrt{4m^2 + 4(n^2 + n - 1)m + 1}$$

(cf. (21)), again providing the Newtonian case ($m = 1$) as being neutrally stable (with bubbles generically approaching ellipsoids at extinction [25, 32]), and the shear-thinning case ($m < 1$) having stable spherical solutions (this time acting in a supercritical fashion for $1/2 < m < 1$). Further, this result suggests that the sphere is unstable to modes with $n < (-1 + \sqrt{12m + 13})/2$, a property that is perfectly analogous to the $N = 2$ case described in the present paper, although the ultimate behaviour of a bubble surface with $N = 3$ for $m > 1$ would be expected to be more complicated (in particular because both prolate and oblate shapes are candidates for the extinction behaviour and because there are two rotational symmetries for $N = 3$, both of which could in principle be lost). There may also exist three-dimensional unstable similarity solutions as m passes through $\frac{1}{3}n(n+1) - 1$ for $n = 3, 4, \ldots$, analogous to ones discussed in sections 3.2 and 5.

Returning to the problem with $N = 2$ dimensions, a slightly more subtle issue concerns what happens if ∂B is not convex so that extinction at multiple points can occur, with the bubble breaking up prior to extinction (we are assuming here that a convex bubble stays convex). The associated transition is discussed in [29] for $m = 1$, but the general case has not been analysed. Finally, we wish to highlight the interfaces illustrated in Figure 4: these are to (Newtonian) ellipses what the solutions of appendix of [35][6] are to parabolas and can be thought of as having rather special status.

Appendix A. Summary of results for Newtonian fluid

The problem (1), (2) and (4) is treated in [32, 33]. We summarise the relevant results here, and refer the reader to these papers for further details.

Appendix A.1. Use of Baiocchi transform

For $m = 1$ we are able to reformulate (1), (2) and (4) with the use of the Baiocchi transform

$$w(x, y, t) = \int_{\omega(x,y)}^{t} p(x, y, t')\, \mathrm{d}t',$$

where the free boundary $\partial\Omega$ is written as $t = \omega(x, y)$. The result is that w satisfies

$$\nabla^2 w = 1 \quad \text{in} \quad B \setminus \Omega(t), \tag{A.1}$$

$$w = \frac{\partial w}{\partial n} = 0 \quad \text{on} \quad \partial\Omega, \quad w = t \quad \text{on} \quad \partial B. \tag{A.2}$$

This formulation has the advantage that time appears as a parameter only, meaning we can solve the problem at the precise moment the bubble vanishes (at the extinction time t_e), and then describe the behaviour of the flow field at times leading up to extinction.

Writing $w(x, y, t_e) = W(x, y) + t_e$ gives

$$\nabla^2 W = 1 \quad \text{in} \quad B \quad \text{with} \quad W = 0 \quad \text{on} \quad \partial B. \tag{A.3}$$

[6] Though, unlike these, they are not exact solutions to the full moving-boundary problem.

The extinction point (x_e, y_e) is then the global minimum of W, and t_e is recovered from $t_e = -W(x_e, y_e)$: these important quantities can be found by solving the linear boundary-value problem (A.3).

We can also extract information about the free boundary from this reformulation. Since

$$w(x, y, t_e) \sim a(x - x_e)^2 + (\tfrac{1}{2} - a)(y - y_e)^2 \quad \text{as} \quad (x, y) \to (x_e, y_e), \quad \text{(A.4)}$$

where a is a constant such that $0 \leq a \leq \frac{1}{2}$, which can be determined from (A.3) and depends on ∂B. In the extinction limit the free boundary approaches the ellipse

$$\left(\frac{2a}{1-2a}\right) x^2 + \left(\frac{1-2a}{2a}\right) y^2 = T^2, \quad \text{(A.5)}$$

where the function $T(t)$ behaves as

$$T \sim \frac{2(t_e - t)^{1/2}}{\log^{1/2}(1/(t_e - t))} \quad \text{as} \quad t \to t_e^-. \quad \text{(A.6)}$$

The aspect ratio of this shrinking ellipse is evidently $(1 - 2a)/2a$. We now explore some further details for instructive special domain shapes.

Appendix A.2. Elliptical domain

One of the simplest non-trivial examples is when ∂B is the ellipse

$$\frac{x^2}{\alpha^2} + y^2 = 1,$$

which has an aspect ratio of α. In this case, not detailed previously, the solution to (A.3) is

$$W = \frac{\alpha^2}{2(1+\alpha^2)} \left(\frac{x^2}{\alpha^2} + y^2 - 1\right).$$

The extinction point (x_e, y_e) is the origin and thus, from $t_e = -W(x_e, y_e)$ and (A.4),

$$t_e = \frac{\alpha^2}{2(1+\alpha^2)}, \quad a = \frac{1}{2(1+\alpha^2)}. \quad \text{(A.7)}$$

The aspect ratio thus evolves from α to $(1 - 2a)/2a = \alpha^2$; the bubble thus increases its aspect ratio, dramatically so when $\alpha \gg 1$, and passes through non-elliptic shapes to approach an ellipse of larger eccentricity than ∂B.

Appendix A.3. Triangular domain

Another straightforward example that has not been detailed previously is when ∂B is the equilateral triangle with sides $y = \pm\sqrt{3}x - 2h/3$ and $y = h/3$. In this case we have

$$W = \frac{1}{4}(x^2 + y^2) + \frac{y}{4h}(y^2 - 3x^2) - \frac{h^2}{27},$$

with the extinction point coinciding with origin and $t_e = h^2/27$, $a = 1/4$, meaning that the bubble is ultimately radially symmetric (as is to be expected on symmetry grounds).

Appendix A.4. Near-circular geometry

In part as a check on our perturbation approach developed above in section 3.1, we apply the Baiocchi transform results of Appendix A.1 to the problem (A.1)-(A.2) for the case in which the fixed boundary ∂B is near-circular and described by $r = 1+\epsilon g(\theta)$, where g is given by (12).

First we must solve (A.3), which is

$$\nabla^2 W = 1 \quad \text{in} \quad 0 \le r < 1 + \epsilon g(\theta) \quad \text{with} \quad W = 0 \quad \text{on} \quad r = 1 + \epsilon g(\theta).$$

Since $\epsilon \ll 1$ we write

$$W = W_0(r) + \epsilon W_1(r,\theta) + \epsilon^2 W_2(r,\theta) + \mathcal{O}(\epsilon^3)$$

to give

$$\nabla^2 W_0 = 1, \quad \nabla^2 W_1 = \nabla^2 W_2 = 0 \quad \text{in} \quad 0 \le r < 1,$$
$$W_0 = 0, \quad W_1 + g(\theta)\frac{\mathrm{d}W_0}{\mathrm{d}r} = 0, \quad W_2 + g(\theta)\frac{\partial W_1}{\partial r} + \tfrac{1}{2}g^2(\theta)\frac{\mathrm{d}^2 W_0}{\mathrm{d}r^2} = 0 \quad \text{on} \quad r = 1.$$

These problems are easily solved, yielding

$$W_0 = \tfrac{1}{4}(r^2 - 1), \quad W_1 = -\tfrac{1}{2}\sum_{n=1}^{\infty} a_n r^n \cos n\theta, \quad W_2 = \sum_{n=1}^{\infty} b_n r^n \cos n\theta,$$

where the where first three b_n are given by

$$b_0 = \tfrac{1}{8}\sum_{j=1}^{\infty}(2j-1)a_j^2, \;\; b_1 = \tfrac{1}{2}\sum_{j=1}^{\infty} j a_j a_{j+1}, \;\; b_2 = \tfrac{1}{8}\sum_{j=1}^{\infty}\{(2j-1)a_j^2 + 2(2j+1)a_j a_{j+2}\}.$$

It follows that the coordinates of the extinction point are given by

$$x_e = \epsilon a_1 + 2\epsilon^2(a_1 a_2 - b_1) + \mathcal{O}(\epsilon^3), \quad y_e = 0, \tag{A.8}$$

and the extinction time is

$$t_e = \tfrac{1}{4} + \epsilon^2(\tfrac{1}{4}a_1^2 - b_0) + \mathcal{O}(\epsilon^3).$$

The result (A.8) implies that perturbing the boundary moves the extinction point away from the origin, with the first-order correction ϵa_1 depending on $g(\theta)$ only through a_1. Thus the 'optimal' choice of the origin is found by setting $a_1 = 0$.

Our Baiocchi transform analysis reveals that the free boundary will approach the ellipse (A.5), where the constant a is found to be

$$a = \tfrac{1}{4} - \tfrac{1}{2}\epsilon a_2 + \epsilon^2 b_2 + \mathcal{O}(\epsilon^3).$$

Thus the aspect ratio of the contracting bubble in the extinction limit is

$$\frac{1-2a}{2a} = 1 + 4\epsilon a_2 + 8\epsilon^2(a_2^2 - b_2) + \mathcal{O}(\epsilon^3), \tag{A.9}$$

which acts as a check on our analysis in section 3.1.

Appendix B. Further details for the linear-stability analysis

In this appendix we treat the problem (1), (2) and (4) for the perturbed circle, which in polar coordinates is

$$\boldsymbol{\nabla}\cdot\left(|\boldsymbol{\nabla}p|^{(1-m)/m}\boldsymbol{\nabla}p\right)=0 \quad \text{in} \quad s(\theta,t)<r<1+\epsilon g(\theta), \tag{B.1}$$

$$p=0, \quad \frac{\partial s}{\partial t}=-|\boldsymbol{\nabla}p|^{(1-m)/m}\left(\frac{\partial p}{\partial r}-\frac{1}{r^2}\frac{\partial s}{\partial\theta}\frac{\partial p}{\partial\theta}\right) \quad \text{on} \quad r=s(\theta,t), \tag{B.2}$$

$$p=1 \quad \text{on} \quad r=1+\epsilon g(\theta), \tag{B.3}$$

with the initial condition $s=1+\epsilon g(\theta)$ at $t=0$, where the function g is defined in (12).

The problem (B.1)-(B.3) is in some respects similar to the Stefan problem analysed by Gammon & Howarth [19], and our working follows theirs (of course, similar issues arise in many other contexts also). We assume the solutions for s and p can be expressed in the form (13), so that to leading order, the (radially-symmetric) problem is to solve

$$\frac{1}{r}\frac{\partial}{\partial r}\left(r\left|\frac{\partial p_0}{\partial r}\right|^{(1-m)/m}\frac{\partial p_0}{\partial r}\right)=0 \quad \text{in} \quad s_0(t)<r<1, \tag{B.4}$$

$$p_0=0, \quad \frac{\mathrm{d}s_0}{\mathrm{d}t}=-\left|\frac{\partial p_0}{\partial r}\right|^{(1-m)/m}\frac{\partial p_0}{\partial r} \quad \text{on} \quad r=s_0(t), \tag{B.5}$$

$$p_0=1 \quad \text{on} \quad r=1, \tag{B.6}$$

with the initial condition $s_0(0)=1$. The first-order problem is

$$\frac{1}{mr}\frac{\partial}{\partial r}\left(r\left|\frac{\partial p_0}{\partial r}\right|^{\frac{1-m}{m}}\frac{\partial p_1}{\partial r}\right)+\frac{1}{r^2}\left|\frac{\partial p_0}{\partial r}\right|^{\frac{1-m}{m}}\frac{\partial^2 p_1}{\partial\theta^2}=0 \text{ in } s_0(t)<r<1, \tag{B.7}$$

$$p_1+s_1\frac{\partial p_0}{\partial r}=0, \quad \frac{\partial s_1}{\partial t}=-\frac{1}{m}\left|\frac{\partial p_0}{\partial r}\right|^{\frac{1-m}{m}}\left(\frac{\partial p_1}{\partial r}+s_1\frac{\partial^2 p_0}{\partial r^2}\right) \text{ on } r=s_0(t), \tag{B.8}$$

$$p_1+g(\theta)\frac{\partial p_0}{\partial r}=0 \quad \text{on} \quad r=1, \tag{B.9}$$

with the initial condition $s_1(\theta,0)=g(\theta)$.

Now, given the leading order solutions (14) and (16), the governing equation (B.7) reduces to

$$\frac{\partial^2 p_1}{\partial r^2}+\frac{m}{r}\frac{\partial p_1}{\partial r}+\frac{m}{r^2}\frac{\partial^2 p_1}{\partial\theta^2}=0,$$

the required solutions of which are of the form (19) with the ϕ_n satisfying the Euler equation

$$\frac{\partial^2\phi_n}{\partial r^2}+\frac{m}{r}\frac{\partial\phi_n}{\partial r}-\frac{mn^2}{r^2}\phi_n=0$$

with the initial condition $\sigma_n=a_n$ at $t=0$. The boundary conditions for the Newtonian case $m=1$ are

$$\frac{\mathrm{d}\sigma_n}{\mathrm{d}t}=-\left(\frac{\partial\phi_n}{\partial r}+\frac{\sigma_n}{s_0^2\log s_0}\right), \quad \phi_n=\frac{\sigma_n}{s_0\log s_0}, \quad \text{on} \quad r=s_0(t),$$

$$\phi_n = \frac{a_n}{\log s_0} \quad \text{on} \quad r = 1,$$

while for $m \neq 1$ they are

$$\frac{\mathrm{d}\sigma_n}{\mathrm{d}t} = -\frac{s_0^{m-1}}{m}\left(\frac{1-m}{1-s_0^{1-m}}\right)^{\frac{1-m}{m}}\left(\frac{\partial\phi_n}{\partial r} - \frac{m(1-m)}{s_0^{1+m}(1-s_0^{1-m})}\sigma_n\right),$$

$$\phi_n = -\frac{(1-m)\sigma_n}{s_0^m(1-s_0^{1-m})} \quad \text{on} \quad r = s_0(t), \quad \phi_n = -\frac{a_n(1-m)}{1-s_0^{1-m}} \quad \text{on} \quad r = 1.$$

In either case the σ_n satisfy

$$\frac{\mathrm{d}\sigma_n}{\mathrm{d}s_0} + \frac{(\nu+\mu_n+m)s_0^{\mu_n} + (-\nu+\mu_n-m)s_0^{-\mu_n}}{ms_0(s_0^{\mu_n} - s_0^{-\mu_n})}\,\sigma_n = \frac{2\mu_n a_n s_0^{\nu+m-1}}{m(s_0^{\mu_n} - s_0^{-\mu_n})}.$$

Appendix C. Further details of the perturbation approach of section 4.2

Here we list details that were not included in section 4.2. Using the rescaling (34), the problem (31)-(33) becomes (first quadrant)

$$\frac{1}{\alpha^2}\frac{\partial}{\partial X}\left(\zeta\frac{\partial p}{\partial X}\right) + \frac{\partial}{\partial Y}\left(\zeta\frac{\partial p}{\partial Y}\right) = 0 \quad \text{in} \quad B \setminus \Omega(t)$$

$$P = 0, \quad \frac{\partial S}{\partial t} = -\zeta\left(\frac{\partial p}{\partial Y} - \frac{\partial s}{\partial X}\frac{\partial p}{\partial X}\right) \quad \text{on} \quad Y = S(X,t),$$

$$p = 1 \quad \text{on} \quad X^2 + Y^2 = 1,$$

where the quantity ζ is the function

$$\zeta(X,Y,t;\alpha) = |\boldsymbol{\nabla} p|^{(1-m)/m} = \left[\frac{1}{\alpha^2}\left(\frac{\partial p}{\partial X}\right)^2 + \left(\frac{\partial p}{\partial Y}\right)^2\right]^{(1-m)/2m}.$$

By writing out (35), the leading-order problem is the quasi-one-dimensional one

$$\frac{\partial}{\partial Y}\left(\frac{\partial P_0}{\partial Y}\right)^{1/m} = 0 \quad \text{in} \quad B \setminus \Omega_0(t),$$

$$P_0 = 0, \quad \frac{\partial S_0}{\partial t} = -\left(\frac{\partial P_0}{\partial Y}\right)^{1/m} \quad \text{on} \quad Y = S_0(X,t),$$

$$P_0 = 1 \quad \text{on} \quad X^2 + Y^2 = 1,$$

while the next order problem is

$$\frac{\partial}{\partial Y}\left\{\frac{1-m}{2m}\left(\frac{\partial P_0}{\partial X}\right)^2\left(\frac{\partial P_0}{\partial Y}\right)^{(1-2m)/m} + \frac{1}{m}\left(\frac{\partial P_0}{\partial Y}\right)^{(1-m)/m}\frac{\partial P_1}{\partial Y}\right\}$$
$$+ \frac{\partial}{\partial X}\left\{\left(\frac{\partial P_0}{\partial Y}\right)^{(1-m)/m}\frac{\partial P_0}{\partial X}\right\} = 0 \quad \text{in} \quad B \setminus \Omega_0(t),$$

$$P_1 + S_1\frac{\partial P_0}{\partial Y} = 0, \quad \frac{\partial S_1}{\partial t} = -\left(\frac{\partial P_0}{\partial Y}\right)^{\frac{1-m}{m}}\left\{\frac{1}{m}\frac{\partial P_1}{\partial Y} - \frac{\partial S_0}{\partial X}\frac{\partial P_0}{\partial X}\right.$$
$$\left. + \frac{1-m}{2m}\left(\frac{\partial P_0}{\partial Y}\right)^{-1}\left(\frac{\partial P_0}{\partial X}\right)^2 + \frac{S_1}{m}\frac{\partial^2 P_0}{\partial Y^2}\right\} \quad \text{on} \quad Y = S_0(X,t),$$

$$P_1 = 0 \quad \text{on} \quad X^2 + Y^2 = 1.$$

Here we are using the notation $B \setminus \Omega_0(t)$ to mean $S_0(X,t) < Y < \sqrt{1-X^2}$ for $0 < X < \Lambda_0(t)$ and $0 < Y < \sqrt{1-X^2}$ for $\Lambda_0(t) < X < 1$.

Acknowledgments

The first author thanks the School of Mathematical Sciences, University of Nottingham, for its kind hospitality during his visit in December 2008 - January 2009, and QUT for additional funding. He also thanks Dr Giles Richardson for helpful comments and discussions. The second author is grateful for the support of the Royal Society and Wolfson foundation.

References

[1] Abramowitz M and Stegun I, 1970 *Handbook of mathematical functions* (New York: Dover)
[2] Alexandrou A N and Entov V 1997 On the steady-state advancement of fingers and bubbles in a Hele-Shaw cell filled by a non-Newtonian fluid, *Euro. J. Appl. Math.* **8** 73–87
[3] Alexandrou A N, Entov V M, Kolganov S S and Kolganova N V 2004 On bubble rising in a Hele-Shaw cell filled with a non-Newtonian fluid, *Euro. J. Appl. Math.* **15** 315–327
[4] Amazigo J C 1974 Fully plastic crack in an infinite body under anti-plane shear, *Int. J. Solids Structures* **10** 1003–1015
[5] Amazigo J C 1975 Fully plastic center-cracked strip under anti-plane shear, *Int. J. Solids Structures* **11** 1291–1299
[6] Andreucci D, Herrero M A and Velázquez J J L 2001 The classical one-phase Stefan problem: a catalog of interface behaviors, *Surv. Math. Ind.* **9** 247–337
[7] Angenent S B and Aronson D G 2003 The focusing problem for the Eikonal equation, *J. Evol. Eq.* **3** 137–151
[8] Angenent S B and Aronson D G 2001 Non-axial self-similar hold filing for the porous medium equation, *J. Amer. Math. Soc.* **14** 737–782
[9] Angenent S B and Aronson D G, Betelú S I and Lowengrub J S 2001 Focusing of an elongated hole in porous medium flow, *Physica D* **151** 228–252
[10] Aronson D G, Van den Berg J B and Hulshof J 2003 Parametric dependence of exponents and eigenvalues in focusing porous media flows, *Euro. J. Appl. Math.* **14** 485–512
[11] Aronsson G and Janfalk U 1992 On Hele-Shaw flow of power-law fluids, *Euro. J. Appl. Math.* **3** 343–366
[12] Atkinson C and Champion C R 1984 Some boundary-value problems for the equation $\boldsymbol{\nabla}.(|\boldsymbol{\nabla}\phi|^N \boldsymbol{\nabla}\phi) = 0$, *Q. J. Mech. Appl. Math.* **37** 402–419
[13] Barenblatt G I, 1996 *Scaling, self-similarity, and intermediate asymptotics* (Cambridge University Press: Cambridge)
[14] Betelú S I, Aronson D G and Angenent S B 2000 Renormalization study of two-dimensional convergent solutions of the porous medium equation, *Physica D* **138** 344–359
[15] Crowdy D G 2005 Quadrature domains and fluid dynamics, in *Quadrature domains and applications, a Harold Shapiro Anniversary volume*, Ebenfelt, Gustafsson, Khavinson and Putinar, eds., (Birkhauser)
[16] Di Benedetto E and Friedman A 1986 Bubble growth in porous media, *Indiana Univ. Math. J.* **35** 573–606
[17] Entov V M and Etingof P I 1991 Bubble contraction in Hele-shaw cells, *Q. J. Mech. Appl. Math.* **44** 507–535

[18] Friedman A and Sakai M 1986 A characterization of null quadrature domains in $\mathbb{R}^N$, *Indiana Univ. Math. J.* **35** 607-610

[19] Gammon J and Howarth J A 1996 The inward solidification of cylinders with a slightly perturbed temperature distribution at the boundary, *Int. Comm. Heat Mass Trans.* **23** 397–406

[20] Gil O and Vázquez J L 1997 Focusing solutions for the p-Laplacian evolution equation, *Adv. Diff. Eqn.* **2** 183–202

[21] Gustafsson B and Shapiro H S 2005 What is a quadrature domain?, in *Quadrature domains and applications, a Harold Shapiro Anniversary volume*, Ebenfelt, Gustafsson, Khavinson and Putinar, eds., (Birkhauser)

[22] Ham F S 1959 Shape-preserving solutions of the time-dependent diffusion equation, *Ql. Appl. Math.* **17** 137-145

[23] Hassager O and Lauridsen T L 1988 Singular behavior of power-law fluids in Hele-Shaw flow, *J. Non-Newtonian Fluid Mech.* **29** 337–346

[24] Hieber C A and Shen S F 1980 A finite-element/finite difference simulation of the injection-molding filling process, *J. Non-Newtonian Fluid Mech.* **7** 1–32

[25] Howison S D 1986 Bubble growth in porous media and Hele-Shaw cells, *Proc. Roy. Soc. Edin.* **102**A 141–148

[26] Karp L 2008 On null quadrature domains, *Comp. Meth. Funct. Theory* **8** 57–72

[27] Kichenassamy S and Véron L 1986 Singular solutions of the p-Laplace equation, *Math. Ann.* **275** 599–615

[28] King J R 1995 Development of singularities in some moving boundary problems, *Euro. J. Appl. Math.* **6** 491–507

[29] King J R and McCue S W 2009 Quadrature domains and p-Laplacian growth, *Comp. Anal. Oper. Theory* **3** 453–469

[30] Kondic L, Palffy-Muhoray P and Shelley M J 1996 Models of non-Newtonian Hele-Shaw flow, *Phys. Rev. E* **54** 4536–4539

[31] Kondic L, Shelley M J and Palffy-Muhoray P 1998 Non-Newtonian Hele-Shaw flow and the Saffman-Taylor instability, *Phys. Rev. Lett.* **80** 1433–1436

[32] McCue S W, King J R and Riley D S 2003 Extinction behaviour of contracting bubbles in porous media, *Quart. J. Mech. Appl. Math.* **56** 455–482

[33] McCue S W, King J R and Riley D S 2003 Extinction behaviour for two-dimensional solidification problems, *Proc. Roy. Soc. Lond.* A **459** 977–999

[34] McCue S W, King J R and Riley D S 2005 The extinction problem for three-dimensional inward solidification, *J. Eng. Math.* **52** 389–409

[35] Richardson G and King J R 2007 The Saffman-Taylor problem for an extremely shear-thinning fluid, *Ql. J. Mech. Appl. Math.* **60** 161–200

[36] Sader J E, Chan D Y C and Hughes B D 1994 Non-Newtonian effects on immiscible viscous fingering in a radial Hele-Shaw cell, *Phys. Rev. E* **49** 420–432

[37] Saffman P G and Taylor G I 1958 The penetration of a fluid into a porous medium or Hele-Shaw cell containing a more viscous liquid, *Proc. Roy. Soc. Lond.* A **245** 312–329

[38] Sakai M 1982 *Quadrature domains*, Lecture Notes in Mathematics, 934, (Springer-Verlag)

[39] Soward A M 1980 A unified approach to Stefan's problem for spheres, *Proc. Roy. Soc. Lond.* A **373** 131–147

[40] Wilson S D R 1990 The Taylor-Saffman problem for a non-Newtonian liquid, *J. Fluid Mech.* **220** 413–425

[41] http://www.maths.ox.ac.uk/∼howison/Hele-Shaw/